Cape Peninsula
University of Technology

USING PHASE CHANGE MATERIALS FOR THERMAL ENERGY STORAGE

by

OKUNDJI KILUMBU

Thesis submitted in fulfilment of the requirements for the degree

Master of Technology: Mechanical Engineering

in the Faculty of Engineering and Built Environment

at the Cape Peninsula University of Technology

Supervisor: Prof. Jasson Gryzagoridis

Bellville campus
November 2020

DECLARATION

I, **OKUNDJI KILUMBU,** declare that the contents of this thesis represent my own, unaided work and that the thesis has not previously been submitted for academic examination towards any qualification. Furthermore, it represents my own opinions and not necessarily those of the Cape Peninsula University of Technology.

Signed: **Date:**

ABSTRACT

The demand for electricity has increased drastically owing to population growth in South Africa. Because of urbanisation, the amount of energy used by residential and commercial buildings is increasing for water heating, space heating, or cooling.

Eskom (the country's power utility) is not coping with the demand; hence a shift to available renewable energy is needed which will alleviate the problem and also result in a clean and efficient way of generating power.

Solar power, converted to electricity or used for water heating, presents a potential solution to the energy demand by the residential and commercial building sectors. The main difficulty in utilising solar energy is that its availability is not continuous, and sometimes unpredictable. In order to alleviate the peak demand time for electricity for heating and cooling, storage of thermal solar energy is a possible solution. A thermal storage unit using phase change materials (PCMs) can be used to supply energy to conventional active space heating and cooling systems at peak energy demand times.

The experimental investigation focused on using a test apparatus to study the melting and solidification processes of paraffin wax as a PCM. The PCM was stored in a vertical annular space between a concentrically placed outer shell and an inner coiled tube through which water, the heat transfer fluid (HTF), was channelled. Various thermo-physical properties have been used to select PCMs due to their high energy storage capacity, availability, being economical, etc. RT25, RT27 and RT35 were selected for this project because of their melting points which are between 15 ºC and 90 ºC and thus applicable to solar energy applications.

Tests were performed for the rate of heat absorbed and released for the three chosen PCMs, measuring the temperature difference across the test section over time for three different flow rates (200, 400 and 600) litres/hour of the HTF. The effect of increasing the flow rate of the HTF was a directly proportional increase to the rate of heat absorbed and released, and inversely proportional to the time taken by the three PCMs tested. The best results were obtained from RT35, with efficiencies of 77%, 82% and 85% for the three respective HTF flow rates, compared with RT27 and R25 in that order.

ACKNOWLEDGEMENTS

I wish to thank:

- My supervisor, Prof. Jasson Gryzagoridis, for his invaluable advice and guidance throughout this research work; My gratitude goes to my family and close friends for their constant encouragement throughout these two years of study.
- My wife, Cadine Nkulu, and children, for all their support, encouragement and love.

DEDICATION

This thesis is dedicated to my parents: my father, the late Daniel Okundji Kilumbu, and my mother, Micheline Kitoto, for their endless love, support and encouragement. I am grateful to my brothers, sisters, and friends for all their love and support during my studies. I am grateful to God our Creator, because only through His love and guidance are we capable of anything.

TABLE OF CONTENTS

LIST OF FIGURES

LIST OF TABLES

LIST OF SYMBOLS

A_S	Cross-sectional area, pipe	[m^2]
C_p	Specific heat of the phase change material	[J/kg ^oC]
D	Diameter of pipe	[m]
D_I	Inside diameter of pipe	[m]
g	Acceleration due to gravity	[m/s^2]
h_r	Head loss	[m]
k	Thermal conductivity	[W/m ^oC]
L	Litre	[L]
LH:	Latent heat of fusion	[J/kg]
m	Mass of material	[kg]
$\dot{m}_{ch}$	Mass flow rate of the HTF during the charging process	[kg/s]
$\dot{m}_{disch}$	Mass flow rate of the HTF during the discharging process	[kg/s]
q	Rate of heat flow	[W]
Q_1	Energy released by the HTF or taken by the PCM during the charging process	[J]
Q_2	Energy gain by the cold HTF during the discharging process or energy discharged by the PCM	[J]
T_1	Inlet temperature of the HTF during charging process	[^oC]
T_2	Outlet temperature of the HTF during the charging process	[^oC]
T_3	Inlet temperature of the HTF during the discharging process	[^oC]
T_4	Outlet temperature of the HTF during the discharging process	[^oC]
T_{pcm}	Melting temperature of the phase change material (PCM)	[^oC]
T_m	Mean temperature	[^oC]
T_{fl}	Fluid temperature	[^oC]
T_s	Surface temperature	[^oC]

ΔT	Temperature difference	[ºC]
t	Time	[sec]
U	Overall heat transfer coefficient	[W/m^2 ºC]
V_1	Average fluid velocity inside the plastic pipe	[m/s]

Greek letters

ρ_i	Density of fluid flowing in the plastic pipe	[kg/m^3]
β	Volumetric thermal expansion coefficient of the PCM	[1/K]
η	Efficiency	[%]
μ	Dynamic viscosity of the PCM	[kg/s. m]
v	Kinematic viscosity	[m^2/s]
ρ	Mass density of the PCM	[kg/m^3]

Abbreviations

DMRE	Department of Mineral Resources and Energy
ERC	Energy Research Centre – University of Cape Town
GDP	Gross Domestic Product
HTF	Heat transfer fluid
HVAC	Heating, ventilation air conditioning
IEA	International Energy Agency
LHS	Latent heat storage
LHTES	Latent heat thermal energy storage
PCM	Phase change material
PPP	Purchasing power parity
PTSC	Parabolic trough solar collector
RT25	Rubitherm phase change material melting at 25 ºC
RT27	Rubitherm phase change material melting at 28 ºC
RT35	Rubitherm phase change material melting at 35 ºC
SHS	Sensible heat storage
TES	Thermal energy storage
TFC	Total final energy consumption
TSU	Thermal storage unit
WRI	World Resources Institute

CHAPTER ONE
INTRODUCTION

1.1 Solar Energy

The sun of our planetary system is considered to be among the cleanest of renewable sources available to mankind, and could be used to alleviate the problems of increasing greenhouse gas emissions (mostly CO_2) and the hike in fossil fuel prices.

According to Sari and Kaygusuz (2006), the sun transmits approximately 30 000 times more energy than required human demand.

South Africa ranks among the regions in the world that receive the highest solar radiation, with good clarity indices and high rates of insolation. The average amount of daily solar radiation in South Africa is 220 W/m². Large parts of the country receive average insolation, over 5 kWh/m² in one day, with the region of the Northern Cape receiving on average over 6 kWh/m² in one day.

Figure 1.1 represents the spread of availability of solar energy over South Africa. Considering that the average modern household daily energy demand is in the region of 30kWh or 108MJ per day, it could be collected and stored in the six to eight hours that is available while the sun is shining; even five hours could conceivably be used to achieve a domestic home's energy requirement (Sharma & Chen, 2009).

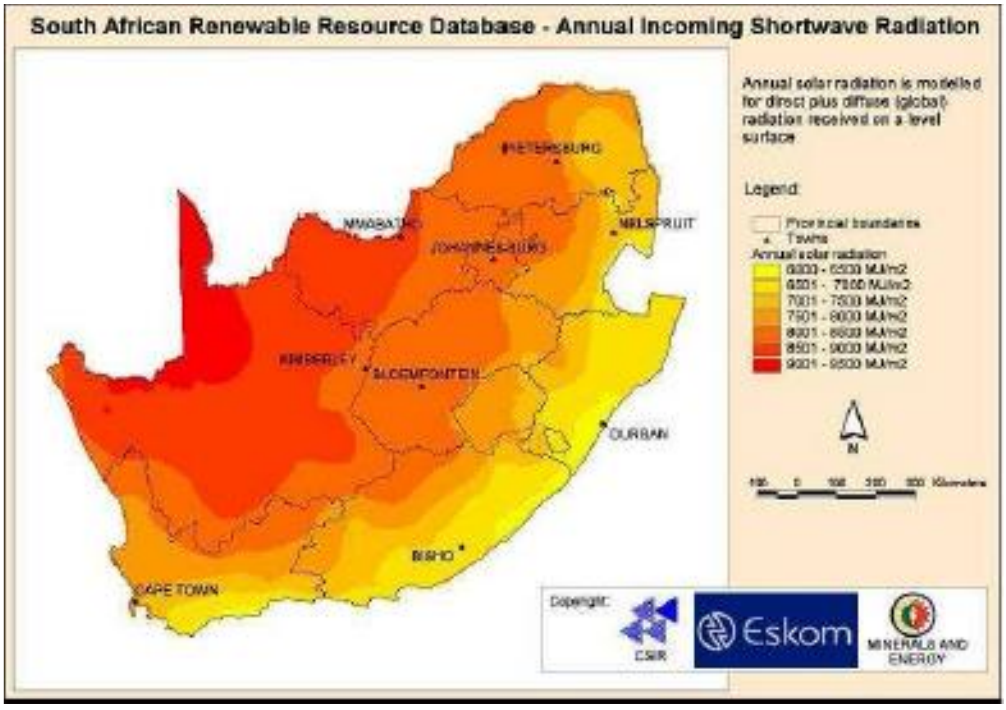

Figure 0.1: Overview of South Africa's annual direct normal irradiation (Fluri, 2009)

There are some problems in collecting solar energy: availability is irregular, and often subject to interruptions due to changes in weather. A possible solution is thermal storage which will release energy for use when the sun is not available. The effective way to utilise the sun's energy (when available) for heating applications is to convert it into thermal energy by using dedicated solar collectors (Fluri, 2009).

The residential and domestic sector of the energy consumed is characterised by the different types of fuel and diverse devices used. The residential sector accounts for 16% of the overall energy consumed, of which 62% is electricity.

Thermal solar energy storage for space heating and cooling and water heating is a viable alternative to the use of electrical energy. Hence, the concept of a system's collecting and storing solar energy, and releasing it through the night for use in the conditioning of space or water heating, has great potential in South Africa (Winkler, 2004).

The successful application of thermal energy storage is dependent to a great extent on the methodology used. Thermal energy storage can either be achieved by:

1. Using sensible heat storage (SHS), where heat energy is stored by increasing the temperature of a medium/material/substance, or by:
2. Latent heat storage, where energy is stored by changing the physical state of the medium/material/substance.

The method of latent heat storage (LHS), which uses a phase change material (PCM), provides a feasible means of storing solar thermal energy. It is characterised by significantly smaller volumes with larger energy storage density and less oscillation of temperature when compared with alternative materials storing only sensible heat (Sarbu & Sebarchievici, 2018).

Thermal energy storage systems can increase the reliability of supply from the power generation of a plant by load smoothing.

1.2 Statement of research problem

The utilisation of available solar power can reduce energy demand from the national electrical grid, but its continuous availability is unpredictable; therefore, a form of thermal storage is in the evening or when there is greater demand.

There is a class of PCMs quite often used in storing solar energy; these technically are grades of paraffin. The material is both non-toxic and safe for the environment. It stores and releases energy within a small temperature change. There is small change in terms of volume of the material between the solid and liquid phase and it is recyclable.

1.3 Aims and objectives

The main objective of this investigation was to evaluate the behaviour of selected PCMs in terms of their characteristics for storing solar energy. To achieve this, the following had to be addressed:

Identify suitable phase change materials for space heating or cooling and water heating that would have high thermal conductivity, high heat of fusion, would melt/solidify in the low-temperature range from 0 to 55 °C, be non-corrosive, commercially easily available and relatively cheap**.**

1.4 Research design and experimental methodology

The development of the solar/thermal energy storage system comprised:

Step 1: Identification of suitable PCM.

Step 2: The design and construction of a thermal energy storage system.

Step 3: Devising an experimental protocol for gathering data from experiments performed in the Department of Mechanical Engineering at the Cape Peninsula University of Technology.

1.5 Scope of the research

The scope of this project was limited to:

Investigating PCMs that have a thermal energy storage potential for low melting temperature. Water was used as the heat transfer fluid.

1.6 Structure of the thesis

Chapter 1: The introduction presents some background to the problem of storage of solar energy.

Chapter 2: Focuses on some of the background related to thermal storage technologies, to finding appropriate material candidates for thermal energy storage (TES), and an efficient configuration of latent heat storage. It also presents various methods of sizing latent heat storage together with a review of related literature on type of materials, heat transfer and applications of PCMs.

Chapter 3: Presents the experimental apparatus and the test procedures used in capturing data during this research work.

Chapter4: Presents the results obtained from the various experiments performed.

Chapter 5: Concludes the thesis by providing a summary of the findings as related to the objectives of this work and final comments on the results obtained.

CHAPTER TWO
LITERATURE REVIEW ON EXISTING THERMAL STORAGE TECHNOLOGY

2.1 Introduction

In this chapter, previous work on thermal storage is presented within two focus areas. The first one covers the thermodynamics of thermal energy storage based on the methods of sensible heating and on the latent heat type, characterised by the phase change of certain materials, together with a small section on thermochemical heat storage systems. The second focus area is a review of the literature on the theoretical and experimental work on the subject.

Establishing the state of the art in existing storage methods, in general, was the aim of this review, particularly in LHS.

2.2 Thermal energy storage methods

Thermal energy storage (TES) refers to the technologies which store energy in a collector to be released later when needed. To increase the effective use of thermal energy equipment, TES systems have this ability (Yang et al., 2019).

TES systems are normally useful for correcting the discrepancy of availability that may exist between the supply (for example, the sun) and the demand for thermal energy at night.

Two main different techniques were considered in this study for TES from the sun: sensible heat storage (when there is a change of temperature) and latent heat storage (LHS) (when there is a change of phase) in the material used.

2.2.1 Energy storage systems using the sensible heat methodology

TES for domestic purposes uses the methodology of sensible heat change in water. A variety of solar domestic and space heating systems use hot water storage containers located either inside or outside buildings. The containments used for water are tanks, pits, caverns, aquifers and lakes (Syed & Hachem, 2019).

In (SHS) systems, as mentioned earlier, energy is stored or released by heating or cooling a liquid or a solid which does not change phase during the process. An SHS system consists of an energy storage material, a container (usually a tank), a pump, and flow control mechanism/valve for the heat transfer fluid involved (HTF). If the material used for energy storage is a liquid, a heat exchanger may be needed to separate the energy storage substance from the HTF. If a solid is used as an energy storage material, it will probably suffice to have it immersed in the HTF.

The amount of energy input required to heat a TES based on sensible heat methodology is proportional to the difference between the outlet and inlet temperatures of the HTF (assuming negligible heat losses to the environment). As shown in Figure 2.1, it can be observed that when the temperature of the storage medium increases, its energy content (internal energy) also increases.

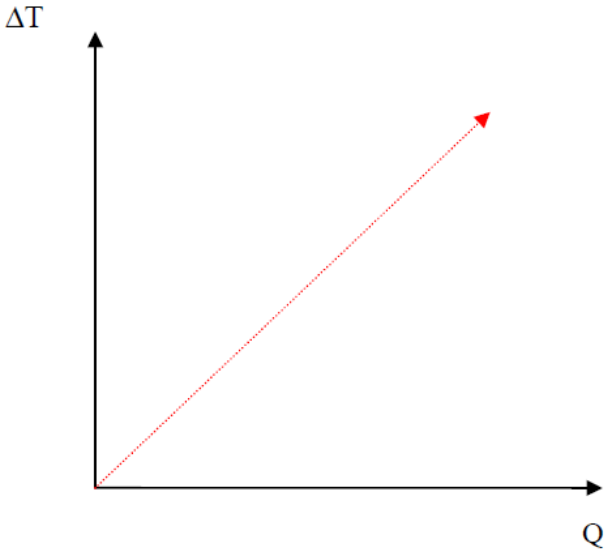

Figure 0.1: Relationship between energy stored and increased temperature

(Duffie & Beckman, 2006)

From first principles of thermodynamics, the quantity of sensible heat released/stored from a solid or liquid (thermal storage substance), under the assumption of negligible heat losses to the environment, is given by the following equation:

$$Q = m\, c_p\, \Delta T = \rho\, C_p\, V \Delta T \qquad (2.1)$$

Where:

C_p: specific heat capacity of the storage material (J/kg °C);

Q: quantity of heat stored (J)

m: mass of heat storage medium/material (kg)

ΔT: temperature change between the maximum and minimum temperatures of the storage material (°C)

ρ: density of the storage material (kg/m^3)

V: volume of storage material (m^3).

Equation 2.1 provides a means to calculate the storage capacity of an SHS system when the extreme temperature difference is known.

In solar air heating systems, the usual energy storage material is a packed bed of small rocks or crushed gravel (Duffie & Beckman, 2006).

The porosity of the bed or the void fraction should be taken into consideration according to Adeyanju and Manohar (2009); the heat stored is given by:

$$Q = C_p \rho (1-\varepsilon) V\Delta T \qquad (2.2)$$

Where

C_p: specific heat capacity of the storage material (J/kg °C)

Q: quantity of heat stored (J)

ε: is the porosity of the packed bed; dimensionless

ΔT: temperature change between the maximum and minimum temperature of the storage material (°C)

ρ: density of the material (kg/m^3)

V: volume of the sensible heat storage material (m^3).

Water is used as one of the best materials/substances to store thermal energy in the form of sensible heat, because it is cheap, has high specific heat, high density and abundant availability. Furthermore, if the water is used as HTF as well, in the solar thermal system,

the need for a heat exchanger is avoided. Table 2.1 lists some materials used for SHS systems.

Table 0.1: Sensible heat storage materials (Sharma et al., 2009)

Medium	Fluid type	Temperature range (°C)	Density (Kg/m^3)	Specific heat (J/Kg°C)
Rock		20	2560	879
Brick		20	1600	840
Concrete		20	1900-2300	880
Water		0-100	1000	4190
Calorie HT43	Oil	12-260	867	2200
Engine oil	Oil	Up to 160	888	1888
Ethanol	Organic liquid	Up to 78	790	2400
Propanol	Organic liquid	Up to 97	800	2500
Butanol	Organic liquid	Up to 118	809	2400
Octane	Organic liquid	Up to 126	704	2400

The SHS system is the simplest form of storing thermal energy when compared with latent heat or thermochemical heat storage systems. However, it has the disadvantage of being larger in size.

The SHS system has been analysed and described by many researchers (Mehling & Cabeza, 2008).

2.2.2 Energy storage systems using the latent heat methodology

Heat that is absorbed and released with the change in the material's phase is known as latent heat, labelled as latent heat of fusion and latent heat of vaporisation. The common phase change to exploit for thermal energy storage is the latent heat of fusion, i.e., the particular phase change from solid to liquid (Wang et al., 2001).

Solid to liquid PCMs present the advantages of smaller volume change during the phase change process and longer lifespan according to Gao et al. (2007), therefore they became the choice for this research.

Among the large number of references related to phase change materials, one can cite Abhat (1981), Lane (1980) and Dinçer and Rosen (2002).

The types of materials used are shown in Figure 2.2. Also shown is the classification and different experimental techniques used to specify the behaviour of PCMs.

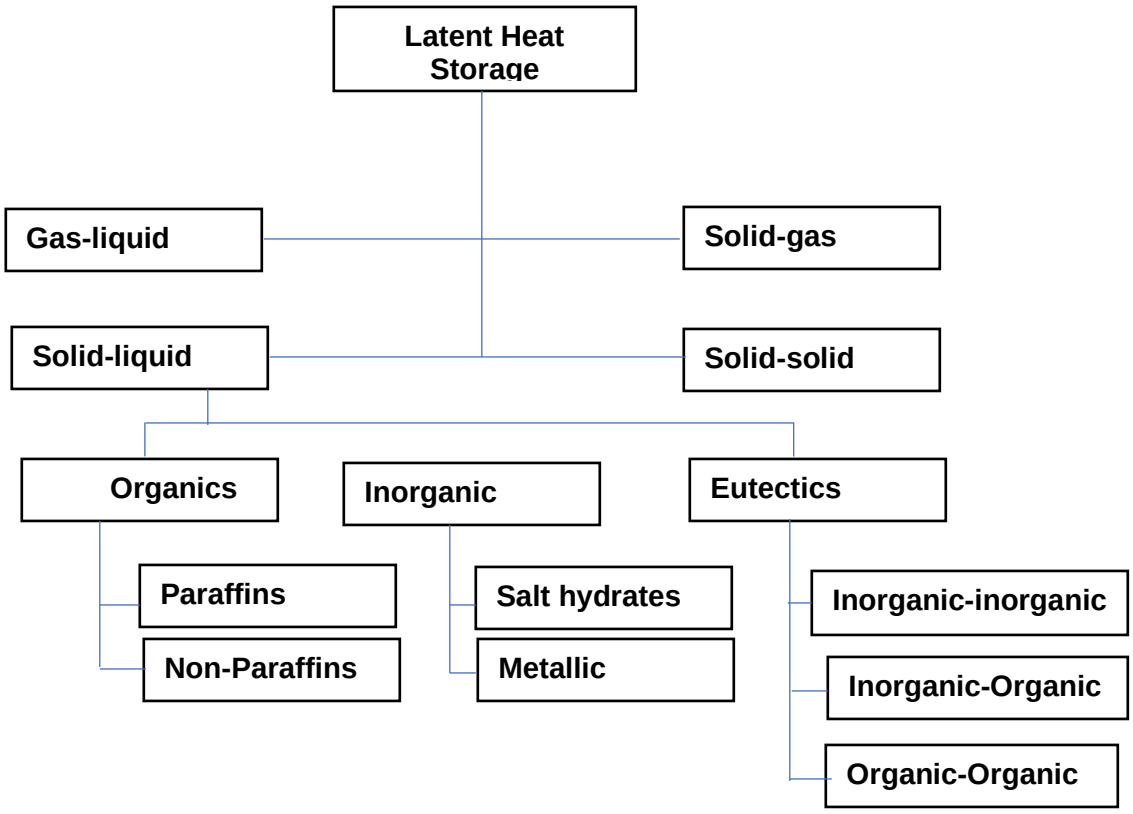

Figure 0.2: Classification of PCMs for LHS materials

(Sharma et al., 2005)

The amount of thermal energy stored in the form of latent heat in a material is calculated by

$$Q = m\ LH \qquad (2.4)$$

where

Q: is the amount of thermal energy stored or released in the form of latent heat (J)

m: is the mass of the material used to store thermal energy (kg)

LH: is the latent heat of fusion(J/kg).

Figure 2.3 shows how the stored energy is a function of changing temperature. The material is in the solid phase at the beginning of the heating period. The heat absorbed is sensible heat just before getting to the melting point of the PCM T_m. Beginning at the melting point, the material goes through a change of state from solid to liquid, and during this process it absorbs heat energy. The temperature of the PCM remains constant; however, the PCM can absorb more heat after this process.

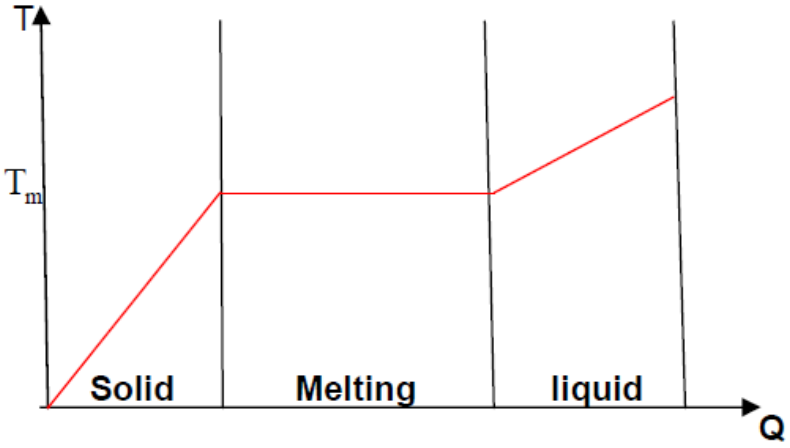

Figure 0.3: Thermal energy stored in a PCM as a function of temperature T (Rubitherm, 2019)

The choice of which PCM is used depends generally on the application. It has to possess desirable thermo-physical, kinetic and chemical properties. The thermo-physical properties

desirable for a PCM and matching melting range for storage capacity are listed by Sarbu and Dorca (2018).

Desirable chemical properties are also required for the choice of a good PCM (De Gracia & Luisa, 2015). PCMs need to be cheap/inexpensive and be fairly easily accessible.

Table 2.2 presents some commercially available PCMs. A conclusion to be drawn from Table 2.2 is that only a few companies are involved in characterisation and marketing of PCMs (Zalba et al., 2003).

Although there are many applications for high, medium and low temperatures, the commercial PCMs available are only in the temperature range of 22 °C to 89 °C.

Table 0.2: Some commercially available PCMs (Zalba et al., 2003)

Commercial Name	Type of product	Melting point(°C)	Heat of fusion(kJ/kg)	Source (Producer)
RT31	Paraffin	31	168	Rubitherm
RT20	Paraffin	22	125	Rubitherm
RT27	Paraffin	28	189	Rubitherm
SP22 A4	Eutectic	22	165	Rubitherm
SP25 A8	Eutectic	25	180	Rubitherm
Clim Sel™ C22	Salt hydrate	22	144	Climator
Clim Sel™ C24	Salt hydrate	24	108	Climator
Clim Sel™ C28	Salt hydrate	28	126	Climator
Clim Sel™ C32	Salt hydrate	32	194.4	Climator
S27	Salt hydrate	27	207	Cristopia
STL27	Salt hydrate	27	213	Mitsubishi Chemical

Table 0.3: Comparisons of organic and inorganic PCMs (Zalba et al., 2003)

ORGANIC	INORGANIC
ADVANTAGES	
Non-corrosive	Great change enthalpy
Non-toxic	Good thermal conductivity
Little or no super cooling	Cheap and non-flammable
Chemically and thermally stable	
DISADVANTAGES	
Lower phase change enthalpy	Undercooling
Low thermal conductivity	Corrosion to most metals
	Phase separation
	Phase segregation
	Lack of thermal stability

2.3 Review of previous work

Reviews of previous efforts were focused on latent heat as the means of thermal storage and provided an insight into new classes of PCMs. The literature review covered both theoretical and experimental works.

2.3.1 Review of theoretical work

Various approaches have been adopted to date with regard to the performance of theoretical models of shell and tube latent (heat) thermal energy storage using multiple PCMs. Figure 2.4 shows the model located in a home. Greater insight into the latent thermal energy storage system can be accessed from the work by Yang et al. (2017).

Their predicted results indicate that there is a peak ratio between different PCMs in order to get the highest rate of thermal energy charge in the latent thermal energy storage system unit. The difference between melting temperatures of several PCMs plays a large part in characterising the performance of the unit.

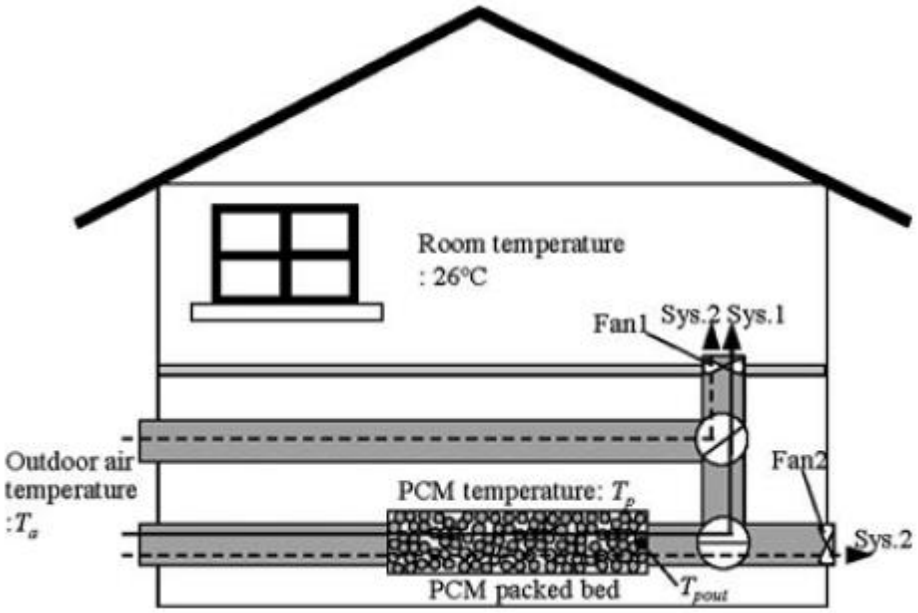

Figure 0.4: Schematic diagram of unit test air supply using PCM packed bed (Takeda et al., 2004)

Takeda et al. (2004) developed a numerical model and investigated experimentally the heat transfer process dominated by conduction inside a latent thermal energy storage unit involving n-Hexacosane as a PCM. The thermal system is made with a triplex concentric tube filled with PCM in the inner channel, with hot HTF flowing through the outer channel during the charging process and cold HTF flowing through the inner channel during the discharging process. Numerical predictions agreed quite well with the experimental results.

Alkilani et al. (2009) conducted a theoretical investigation to predict the output air temperature due to the thermal energy discharge process from a unit consisting of an inline single row of cylinders which contained a PCM (paraffin wax) with a mass fraction 0.5% of aluminium powder in order to improve the heat transfer. Increasing the mass flow rate has the effect of decreasing the outlet temperature of the air according to Speyer (1994), who gave a good overview, but also according to Dinçer and Rosen (2010), who focused their studies on thermal analysis methods for PCMs (Mettawee & Assassa, 2007).

According to Flaherty (1971), there are certain techniques such as conventional, scanning and thermal analysis used to analyse phase change. Satyanarayana et al. (1986) also conducted similar studies investigating the characterisation of hydrocarbons, natural waxes, and petroleum products.

Zhu et al. (1999) reported on a study whereby they discovered a simple method to determine phase change.

Marin et al. (2003) reported results of a study on phase change and developed an evaluation procedure to determine the properties of specific heat and enthalpy. The thermal conductivity of PCMs around phase change temperatures can be determined by a one-dimensional conduction heat transfer in a cylinder (Delaunay & Carré, 1982).

2.3.2 Review of experimental work

Early applications of PCMs for thermal storage used for heating and cooling systems in buildings are described in the literature (Lane, 1986). Building structural components can be used for thermal storage. Safety is most important when using PCMs in buildings, and to avoid fires, possible fire-retardant additives (organic halogenous compounds) could be used (Joulin et al., 2009).

Using PCMs impregnated into building materials is very promising, according to Fang et al. (2012), because it increases the thermal mass of the PCMs.

Another promising concept has been proposed, known as free-cooling, where PCMs are used to store the coolness from ambient air during the night, and used as a relief from the indoor ambient air during the day (Thakare & Deshmukh, 2018).

The University of South Australia has investigated this type of system for buildings, where there is an overproduction of heat during the day, as in offices, schools and shopping centres (Hed et al., 2004).

A shell tube heat exchanger system has been used to investigate the behaviour of melting and solicitation of paraffin wax as PCM (Akgün et al., 2007).

2.3.3 Roof integrated solar heating system with glazed collector

A model of a roof integrated solar heating, combined with PCM located in the thermal storage which allows the setup to operate in three weather conditions (sunny day, night and winter season) is shown in Figure 2.5 (Saman & Belusko, 1997).

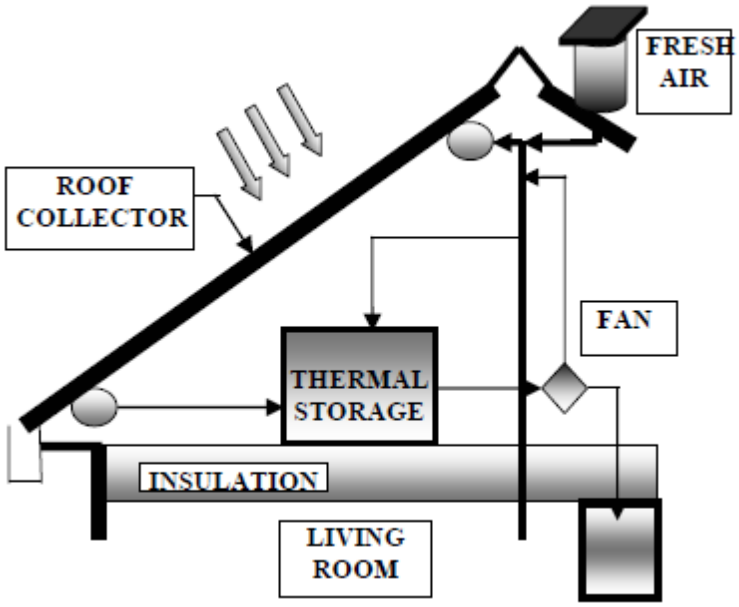

Figure 0.5: Solar collector using thermal storage (Saman & Belusko, 1997)

2.4 Summary

Two basic methods of thermal storage were reviewed in this chapter: Sensible Heat Storage and Latent Heat Storage. A motley of different applications related to these storage methods was presented.

From the literature review on the subject, different mathematical models used to solve phase change problems were identified. Some analytical approximation methods for an LHS, according to Shamsundar (1992), Kang et al. (1999), and Alexiades and Solomon (1993), were judged to be useful in this research.

CHAPTER THREE
DESIGN AND CONSTRUCTION OF THE APPARATUS AND EXPERIMENTAL PROTOCOL

3.1 Introduction

This chapter describes the experimental apparatus constructed and the procedure followed to evaluate the behaviour of the chosen PCM materials for storing and recovering heat energy. It was assumed that the heat energy was harvested through solar collectors. A diagram of the test unit system is presented in Figure 3.1.

The apparatus was required to test the behaviour of three different PCM paraffins (RT25, RT 28, RT35) for their rate of heat absorption and release. This was accomplished by measuring the temperature difference across the test section over a certain time during the charging/discharging process of the PCMs, for different mass flow rates of the HTF (heat transfer fluid).

The test apparatus consists of three fundamental components as listed below and depicted in the schematic diagram, Figure 3.1 and photograph, Figure 3.2.

The fluid flow system consists of piping to convey the HTF, the electrical urn to heat the HTF, the cold HTF storage tank, the circulating pump, the flow metering device, and the TES/heat transfer unit.

The TES unit comprises a heat exchanger (heat transfer shell-helical tube configuration) with the PCM filling the cylindrical container, and the hot HTF flowing in the coil tube system during charging (melting of the PCM) and cold HTF flowing during discharging.

The test apparatus temperature measurement system consists of eight thermocouples (type K), thermocouple switch, and fluke multimeter (data logger system).

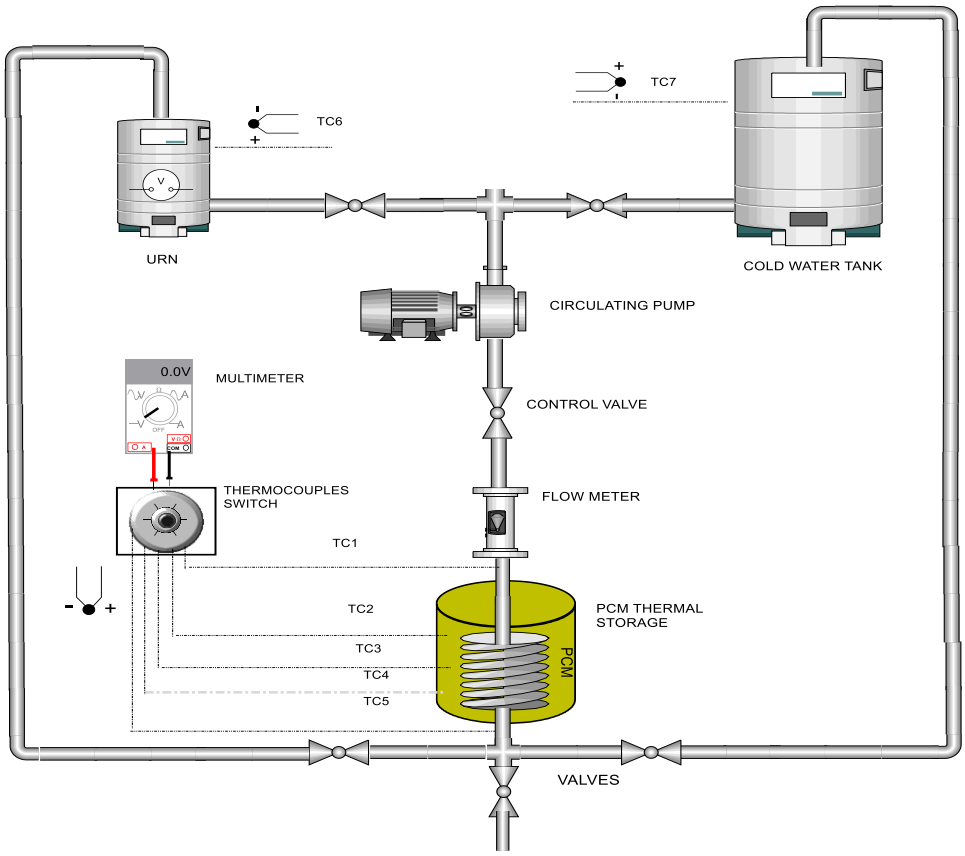

Figure 3.1: Schematic diagram of the apparatus

Figure 3.1 shows the design experimental setup. Generally, it consists of a constant temperature water bath, a circulation pump, and the PCM storage test section with the locations of the thermocouples.

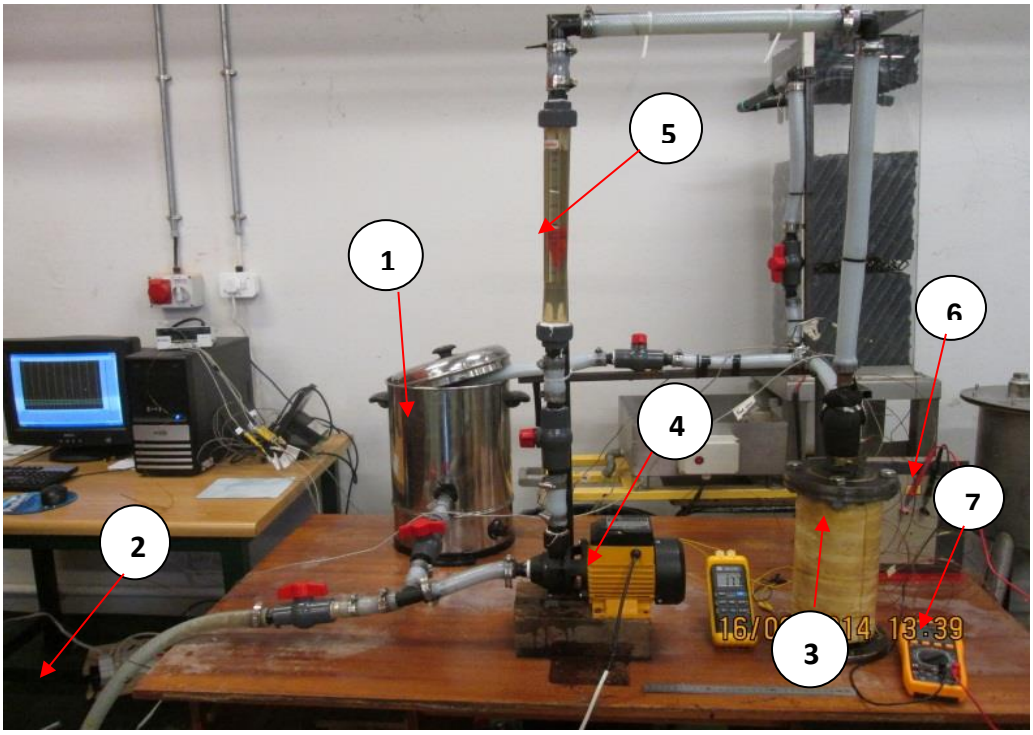

Figure 3.2: Photograph of the experimental setup

The experimental facility used in this study is shown in Figure 3.2. (1) Hot water storage tank, (2) cold water storage tank, (3) PCM heat storage tank (4) centrifugal pump, (5) rotameter, (6) thermocouple switch, and (7) readout data logger system.

3.2 The fluid flow system

The HTF flow section consists of two circuits, the main circulating circuit and the by-pass circuit. The main circuit consists of a flow meter at the exit of the PCM thermal storage unit, after which the HTF is routed via the circulating pump to the urn (the constant temperature tank), a flow adjustment valve allowed for experiments at various HTF flow rates.

Figure 3.3: Salton stainless-steel urn – 16 Litre

In order to heat the HTF (water) to a specified temperature, a 16-litre urn was used as shown in Figure 3.3. The urn chosen was a Salton stainless-steel urn with variable thermostatic control. The urn's tap was replaced with a plastic adaptor in order to connect to the piping used in the fluid flow system.

The cold-water storage tank's capacity was 100 litres. A 1500W centrifugal pump shown in Figure 3.4 was used during the charging cycle (to pump the hot HTF from the urn to the PCM thermal storage unit, then back to the urn) and during the discharging cycle (to pump the HTF from the cold-water storage tank to the PCM thermal storage unit and then to the drain storage tank.

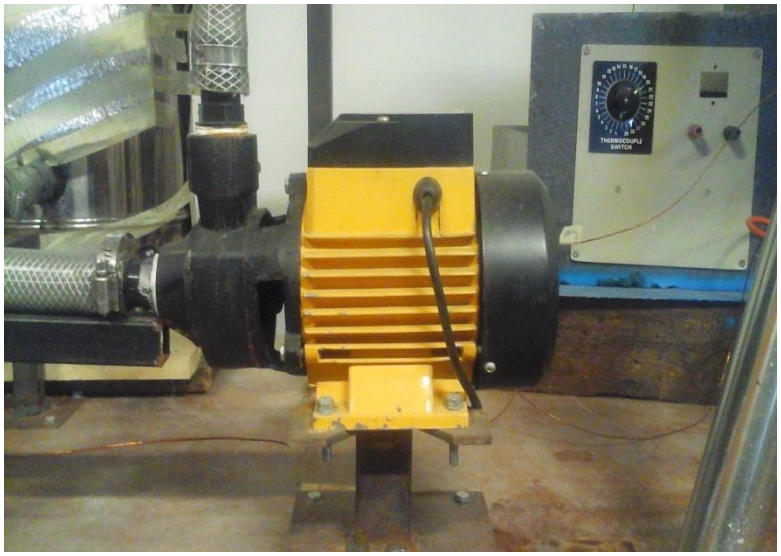

Figure 3.4:Circulating pump

3.2.1 Flow meter (rotameter)

Table 3.1: Pump with motor

Pump with motor type AT3125 E synchronous motor	
Power [W]	1500
Voltage [V]	220–240
Current [A]	0.7–1.2
Power factor	0.68
Frequency [Hz]	60
Rotational velocity [rpm]	1340

In order to measure the flow rate of HTF which was water, a rotameter was used, installed after the pump as shown in Figure 3.5.

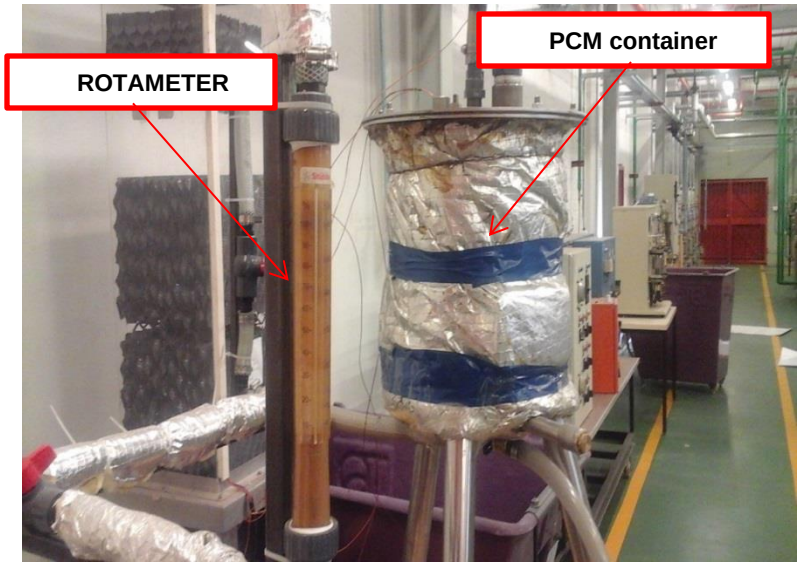

Figure 3.5: Rotameter and PCM thermal storage container

3.3 The PCM thermal storage container

The PCM thermal storage container was manufactured as a cylindrical section 300 mm dia. from a 3mm thick stainless-steel sheet. The closed end of this section was made from a 2mm thick stainless-steel sheet. An Φ180x12mm thick flange was butt-welded to the open end of the cylindrical section to secure the removable end-cap to the storage container. The outside surface of the PCM thermal storage container was insulated with glass wool of 30mm thickness to reduce heat losses to the surroundings as shown in Figure 3.5.

3.3.1 Heat exchanger helical coiled tubing

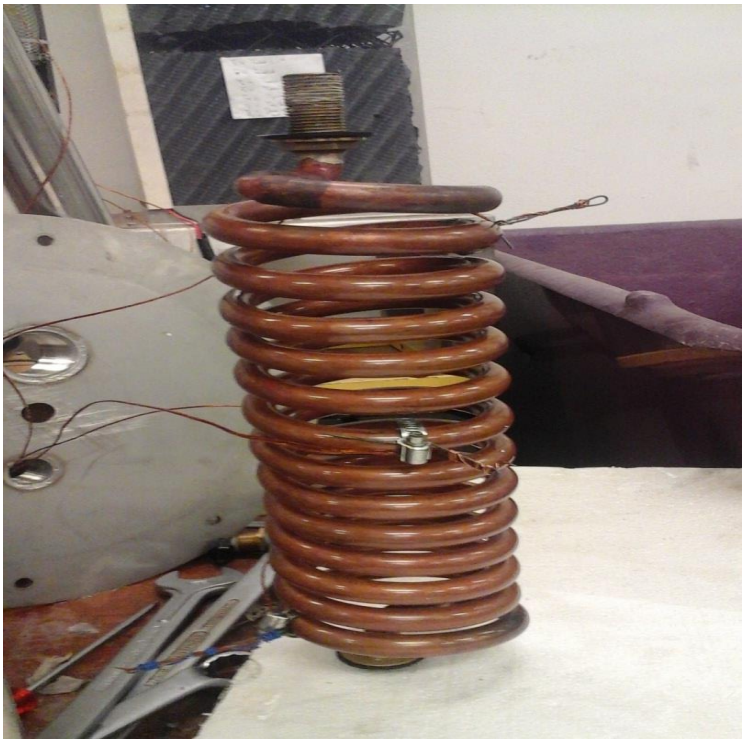

Figure 3.6: Heat exchanger helical coiled copper pipe

The heat exchanger is made of Ø20x2mm thick, coiled copper tubing. This section is placed inside the cylindrical PCM thermal storage container. The spiral design (Figure 3.6) and schematic diagram (Figure 3.7) are shown above and overleaf.

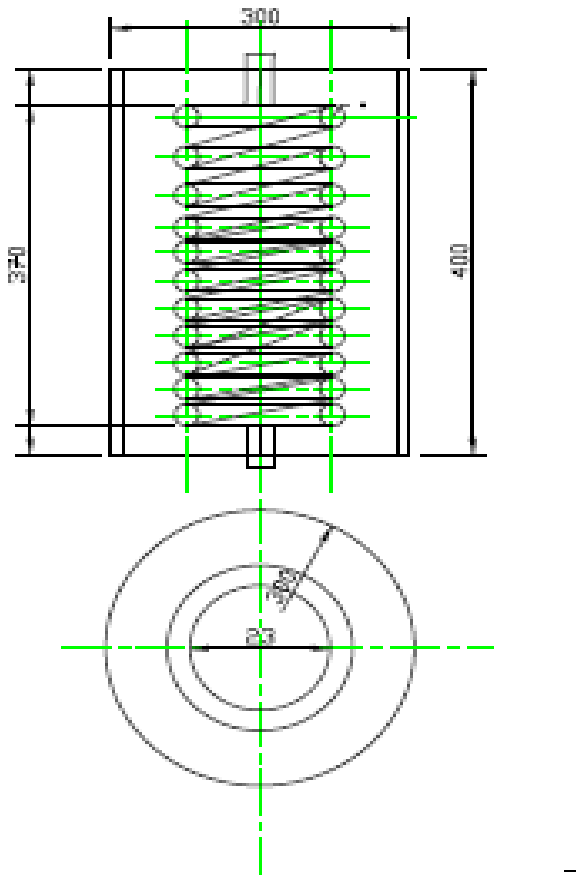

Figure 3.7: Schematic diagram of heat exchanger helical coiled copper pipe

3.4 Temperature measurements

The instrumentation used to measure the temperatures in this study: (1) eight thermocouples were used to evaluate the temperatures of the PCM in the storage container as well as of the water at different locations inside the main storage tank, inlet and outlet heat exchanger system, (2) a data-acquisition system to record temperatures.

3.4.1 The thermocouples

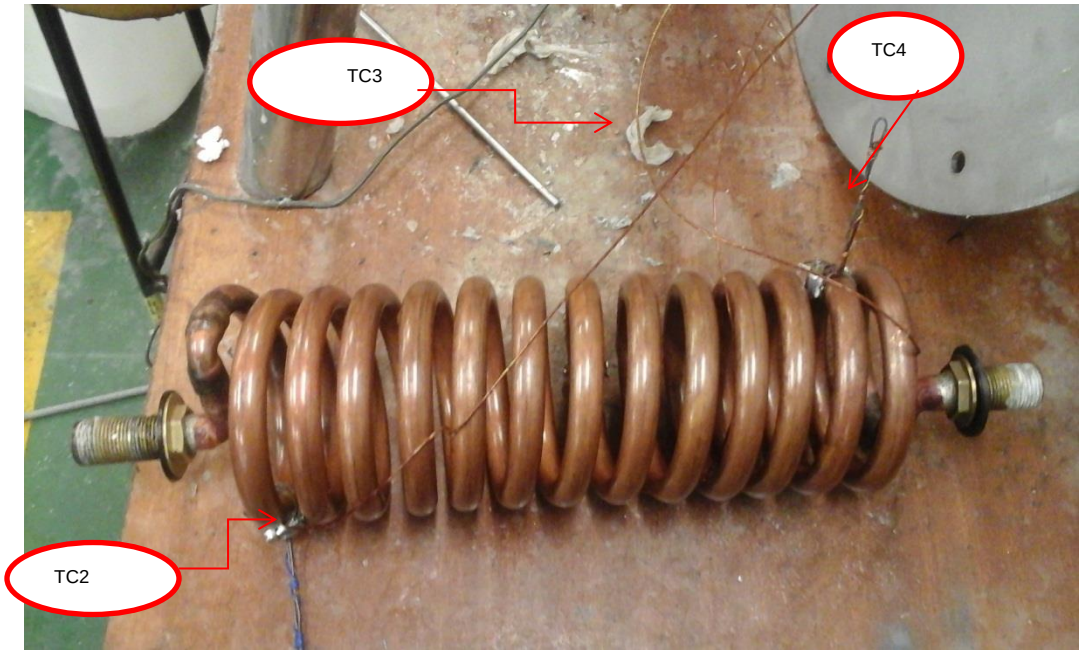

Figure 3.8: Thermocouple location inside the PCM storage container

The temperatures of the PCM in the thermal storage container at different locations were measured using K-type thermocouples. K-type thermocouples (copper and constantan) have an accuracy of ±0.5 ºC in their operating temperature range of -184 ºC to +371 ºC. The thermocouples used in the experimental rig were successfully tested for functionality in a bath of crushed ice and water for the zero ºC degrees mark and in boiling water (at atmospheric pressure) for the 100 ºC mark, prior to being placed in their positions.

Figure 3.8 shows the locations of the thermocouples inside the PCM storage container. The thermocouples and their locations were positioned as follows:

- Three thermocouples (TC_2, TC_3 and TC_4) were installed inside the PCM thermal storage container at different vertical levels in order to measure the instantaneous temperatures of HTF during the charging or discharging processes.
- Two thermocouples (TC1 and TC5) were installed on the surface of the pipe as it entered and exited the PCM thermal storage container respectively, in order to measure the inlet and outlet temperatures of the HTF.
- Two thermocouples (TC6 and TC7) were installed inside the urn at different heights, in order to measure and ensure constancy of the average temperature of the water.

3.4.2 Thermocouple switch and multimeter

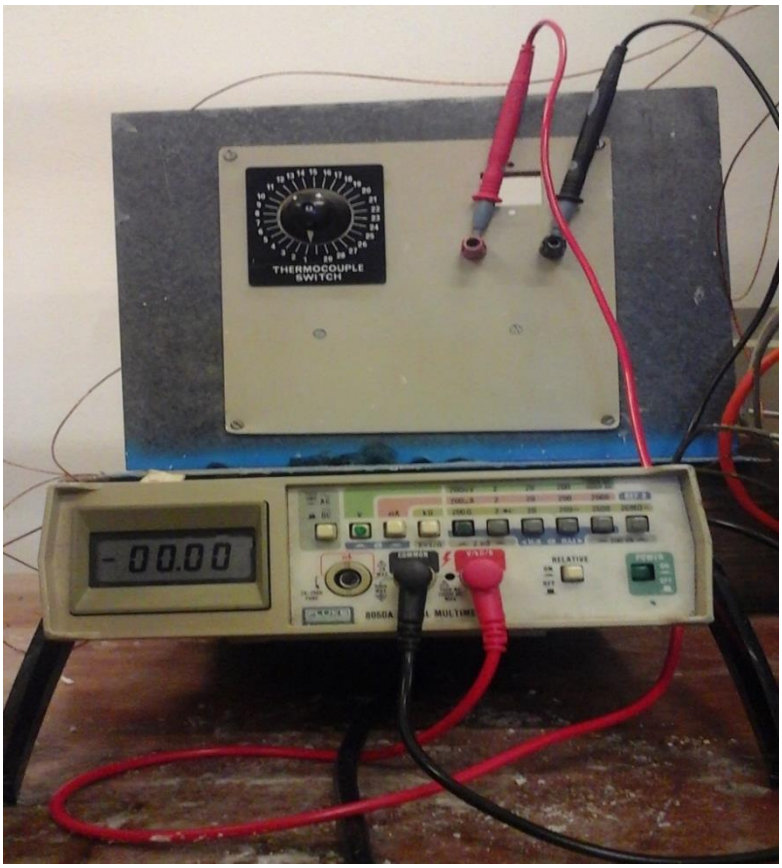

Figure 3.9: Thermocouple switch and multimeter

The data acquisition unit used for displaying the output of the thermocouples (millivolts) was a Fluke multimeter. The millivolt reading displayed on the Fluke multimeter was translated to temperature (^{0}C) using a Fluke thermocouple voltage to temperature calculator. Excel spreadsheets were used to record the temperature data which were logged every 10 minutes; all thermocouples were connected to the multimeter via a switch. Figure 3.9 shows a photographic view of the thermocouple switch and Fluke multimeter.

3.5 Identification of the heat storage material

The new generation of ecological heat storage takes advantage of the behaviour of PCMs, i.e., the process of a material's phase change between solid and liquid (solidifying and melting) to release or store quantities of thermal energy at a nearly constant temperature.

3.5.1 Choice of PCMs

The PCMs' changing phase during a thermal reading of 20 °C to 50 °C was sought. PCMs with this melting temperature range are paraffins, fatty acids, salt hydrates and eutectic mixtures. Fatty acids and salt hydrates were eliminated owing to their corrosive effects. Salt hydrates also have problems, such as melting incongruently and sub-cooling. Paraffins were chosen as the best candidates for PCMs for this project because of their high storage capacity; they are non-toxic, non-corrosive and they are thermally and chemically stable.

Properties of Rubitherm PCMs:

- High thermal energy storage capacity
- Heat storage and release take place at relatively constant temperatures
- No super-cooling effects
- Long-life product, with stable performance through the phase change cycles
- Ecologically harmless and non-toxic
- Chemically inert
- Melting temperature range between approx. 4 °C and 100 °C

From the available PCMs (from Rubitherm), only RT25, RT27 and RT35 were selected for this project because of their melting points which are between 15°C and 90 °C and thus suited to solar energy applications (Farid, et al., 2004).

Table 3.2 shows the selected data for all three chosen PCMs (RT25, RT27, and RT35), supplied by Rubitherm Germany (Rubitherm, 2019). Briefly, both RT27 and RT35 have the highest volumetric storage density (134 MJ/m^3) and moderate latent heat of fusion. RT25 has the lowest volumetric storage density (119 MJ/m^3) and latent heat of fusion. All three PCMs have low volume expansion (10%), which is desirable, and low thermal conductivity (0.2 W/m °C), which is undesirable.

Table 3.2: Properties of technical grade paraffin Ributherm RT25, RT27, and RT35

Description	RT25	RT27	RT35
Melting temperature of the PCM [°C]	26	28	35
Latent heat of fusion [kJ/kg]	180	179	157
Density of the PCM (liquid phase) [kg/m^3]	1.38	0.75	0.76
Specific heat of the PCM (solid phase) [kJ/kg °C]	2.5	1.8	2.4
Thermal Expansion Coefficient [%]	10	10	10
Heat conductivity (both phases) [W/m °C]	0.6	0.2	0.2

3.6 Experimental procedure

The experimental apparatus designed and constructed as described in the sections above was employed to study the charging and releasing processes of the PCMs (RT25, RT28,

and RT35). This was accomplished for different flow rates all at an identical inlet temperature of the 'charging' HTF.

3.6.1 Operating procedure when charging the system

The urn was switched on to heat the HTF to the required charging inlet temperature. The pump (on the charging line) was turned on, and the rotameter was rectified at the required HTF flow rate.

The HTF flows from the urn to the PCM thermal storage container (vertically from top to bottom) and as a result, heat is transferred from the charging HTF to the PCM. The temperature of the HTF decreases until it leaves the container back to the electrical urn, while the temperature of the PCM increases.

Eventually thermal steady state was reached between the temperature of the HTF and the PCM in the heat storage, and the charging mode was terminated.

Table 3.3: Temperature conditions for the charging of the different PCMs

	Flow rate [L/hr]	Ambient temperature [°C]	Inlet temperature of HTF [°C]	Initial store temperature [°C]
Charging process	**600**	**21**	**68–70**	**23**
Charging process	**400**	**20.2**	**68–70**	**23**
Charging process	**200**	**19.9**	**68–70**	**23**

3.6.2 Operating procedure when discharging the system

Similar to 'charging' the system, the pump on the discharging mode was adjusted to the same flow rate; this was done by utilising the rotameter and throttling valve.

Coldwater is pumped from the cold-water storage container to the PCM thermal storage container. The HTF flows vertically from top to bottom through the main PCM thermal storage container and heat is transferred from the PCM to the cold water. The discharging

process was continued until heat steady state was reached between the temperature of the HTF and the PCM in the thermal storage container.

Table 3.4: Temperature conditions for the discharging of the different PCMs

	Flow rate [L/hr]	Ambient temperature [°C]	Inlet temperature of HTF [°C]	Initial store temperature [°C]
Discharging process	**600**	**21.3**	**16–17**	**55**
Discharging process	**400**	**21.6**	**16–17**	**55**
Discharging process	**200**	**22.7**	**15–17**	**55**

CHAPTER FOUR
RESULTS AND DISCUSSION

4.1 Introduction

This chapter, following a brief analysis of the heat transfer that takes place during the PCM phase change (solid to liquid and the reverse), presents the results of the experimental work undertaken in storing and recovering heat energy.

The results obtained, using the three PCMs, are presented and a comparison between them as suitable thermal storage materials is made in terms of their energy storage when charging them, and of course their discharging characteristics when recovering the stored energy.

The comparison (between the chosen PCMs) is based on the results from the parametric tests performed when varying the operating conditions on the thermal energy storage unit/ housing containing an individual PCM. The tests consisted of observing and recording the behaviour of the HTF during the period of charging/storage and discharging/recovery of the heat energy onto or from the PCMs, for three volumetric flow rates.

4.2 Determination of the heat transferred during the PCM phase change

To determine the heat, transferred during the charging mode from (hot water to PCM) and the discharging mode from (PCM to cold water), it was assumed that most of the heat transferred to or from the PCM was at melting/solidification temperature in the form of latent heat.

In developing the heat transfer model for the thermal energy storage unit, the following assumptions were made:

- The thermophysical properties of the liquid and the solid phase of the PCM remain constant.
- No heat exchange occurs on the environment and the thermal storage unit.

4.2.1 Heat released by the water during the charging process

The total amount of heat transferred (Q_1) from the HTF (water) that flowed inside the copper tube coil to the PCM stored in the container was calculated (as shown in Equation 4.1), based on the summation of the products of the mass flow rate of the water ($\dot{m}_{ch}$), the specific heat of water (Cp), the difference in inlet and outlet temperatures of the water as it enters and leaves the copper tube coil ($T_1 - T_2$) and the small time (*Time*) increment that it took for the recording of the individual or each temperature difference during the entire process (Amori & Sherza, 2013).

$$Q_1 = \sum (\dot{m}_{ch} Cp(T_1 - T_2).Time) \quad \textbf{(4.1)}$$

4.2.2 Heat taken up by the water during the discharging process

In a similar manner to described in the section above (4.2.1), the heat energy released during the discharging process from the PCM to the HTF (cold water) is given by:

$$Q_2 = \sum (\dot{m}_{disch} Cp(T_4 - T_3).Time) \quad \textbf{(4.2)}$$

The quantities in Equation 4.2 are identical to those described for Equation 4.1, with the exception of the difference between the outlet and inlet water temperatures ($T_4 - T_3$) respectively.

4.2.3 The behaviour of the HTF during the charging/storing of thermal energy on the PCM

Following are the experimental results for the charging process with the water's inlet temperature of 70 ℃. Figures 4.1 to 4.3 show the behaviour of the temperature difference of the water for each PCM grouped together as they were tested.

The experiments of energy charging/storing on the PCM were performed with three different flow rates and the same constant inlet temperature of the water. Results were

obtained for the mass flow rates of water being equivalent to volumetric flow rates of 200, 400, and 600L/hr, all with the same constant inlet temperature of 70 °C.

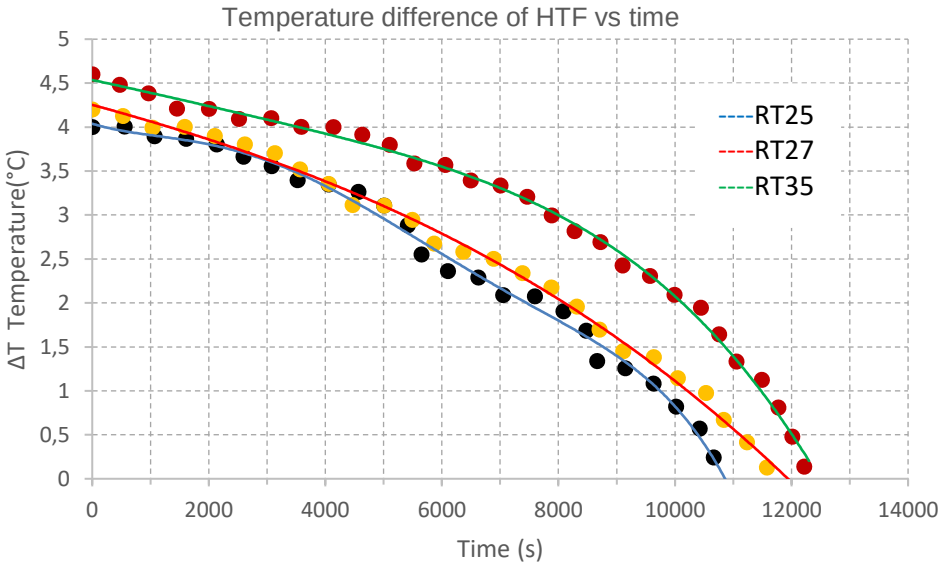

Figure 4.1: Charging process–temperature change of water for each PCM at a flow rate of 200L/hr

Figure 4.1 shows that the time to complete the charging process for each PCM (RT25, RT27, and RT35) at a flow rate of 200 L/hr was 180, 195, and 205 minutes, respectively.

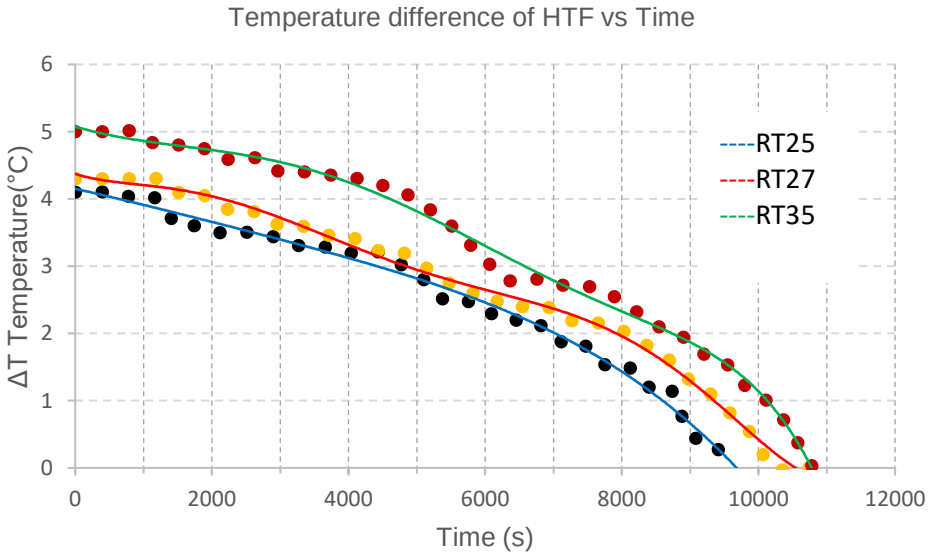

Figure 4.2: Charging process–temperature change of water for each PCM at a flow rate of 400L/hr

Figure 4.2 shows that the time to complete the charging process for each PCM (RT25, RT27 and RT35) at a flow rate of 400 L/hr was 160, 180, and 175 minutes respectively.

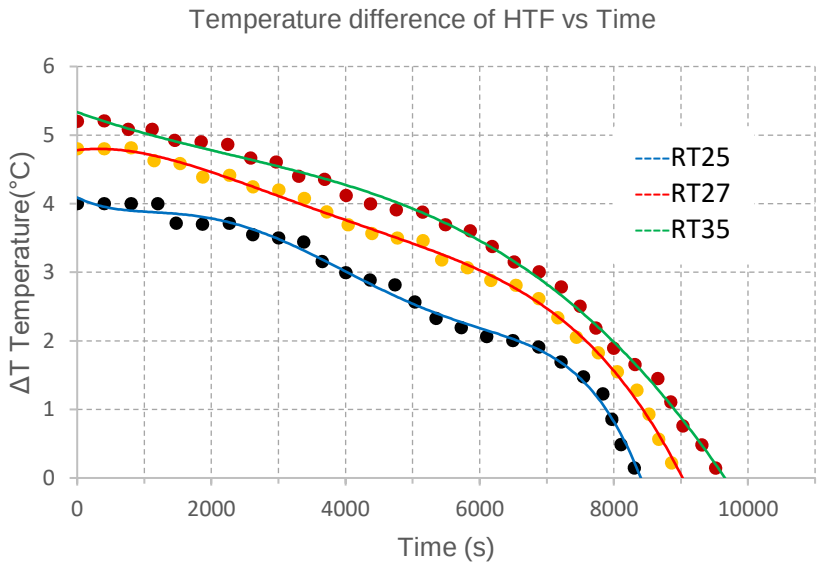

Figure 4.3: Charging process–temperature change of water for each PCM at a flow rate of 600L/hr

Figure 4.3 shows that the time to complete the charging process for each PCM (RT25, RT27, and RT35) at a flow rate of 600 L/hr was 140, 150, and 160 minutes respectively. In comparing Figures 4.1 to 4.3, it confirms that an increase in the flow rate of the water has an inverse effect (as expected) on the time to complete the charging process, that is, the higher the flow rates the quicker the charging process. Table 4.1 shows the time required to charge or store thermal energy on the chosen PCMs at different volumetric flow rates and constant initial temperature of the HTF (water).

Table 4.1: Time to charge/store thermal energy at different flow rates and constant initial inlet temperature of the HTF (water)

	The time to complete the charging process		
	@ 200L/hr	**@ 400L/hr**	**@ 600L/hr**
HTF inlet temperature	**70 °C**	**70 °C**	**70 °C**
RT25 Time (minutes)	180	160	140
RT27 Time (minutes)	195	175	150
RT35 Time (minutes)	205	180	160

4.3 The behaviour of the HTF during the discharging of thermal energy from the PCM

This section deals with the behaviour of the water during the discharging/releasing of thermal energy from the chosen PCMs (RT25, RT27, and RT35).

The experiments performed used cold water directed to flow through the copper coil located in the thermal storage container. The discharging experiments were conducted with the same water flow rates, i.e., 200, 400, and 600 L/hr. The discharging process shown in Figures 4.4 to 4.6 began after the completion of the charging process. The inlet temperature of the cold water was constant at 18 °C, with an initial temperature of the PCM at 45 °C. The PCM temperature was 25 °C at the end of the discharging process.

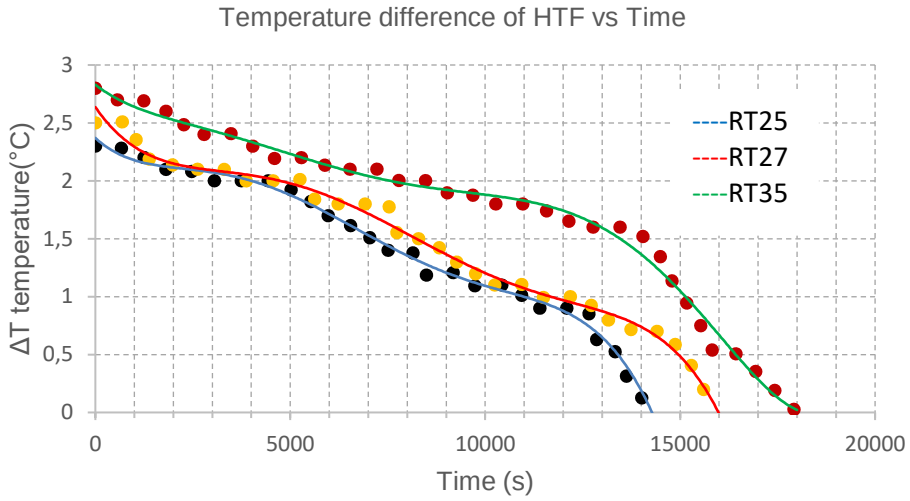

Figure 4.4: Discharging process–temperature difference of the water for each PCM at a flow rate of 200L/hr

Figure 4.4 shows the temperature difference vs. time of the water (flowing at a rate of 200 L/hr) as it recovered energy from each individual PCM. The time recorded for each PCM (RT25, RT27, and RT35) to complete the discharging process was 180, 195, and 205 minutes respectively.

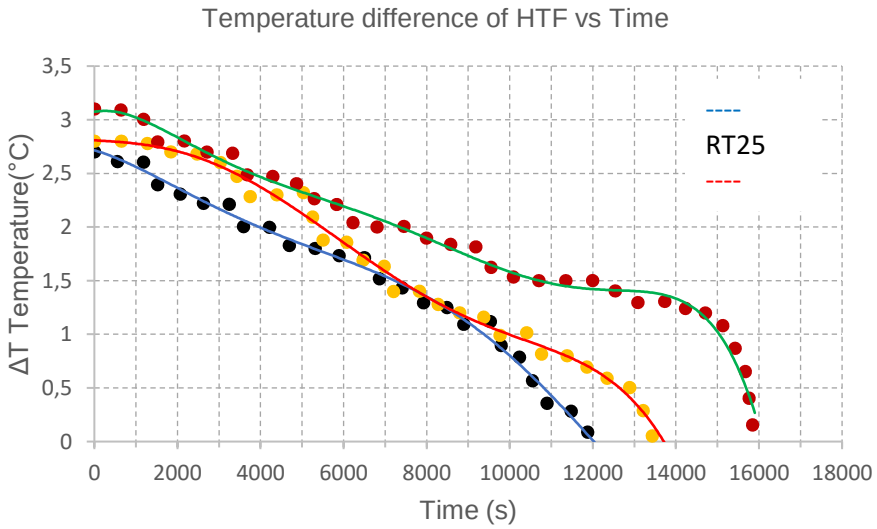

Figure 4.5: Discharging process–temperature difference of the water for each PCM at a flow rate of 400L/hr

Figure 4.5 shows the temperature difference vs. time of the water (flowing at a rate of 400 L/hr) as it recovered energy from each individual PCM. The time recorded for each PCM (RT25, RT27 and RT35) to complete the discharging process was 160, 175, and 180 minutes, respectively.

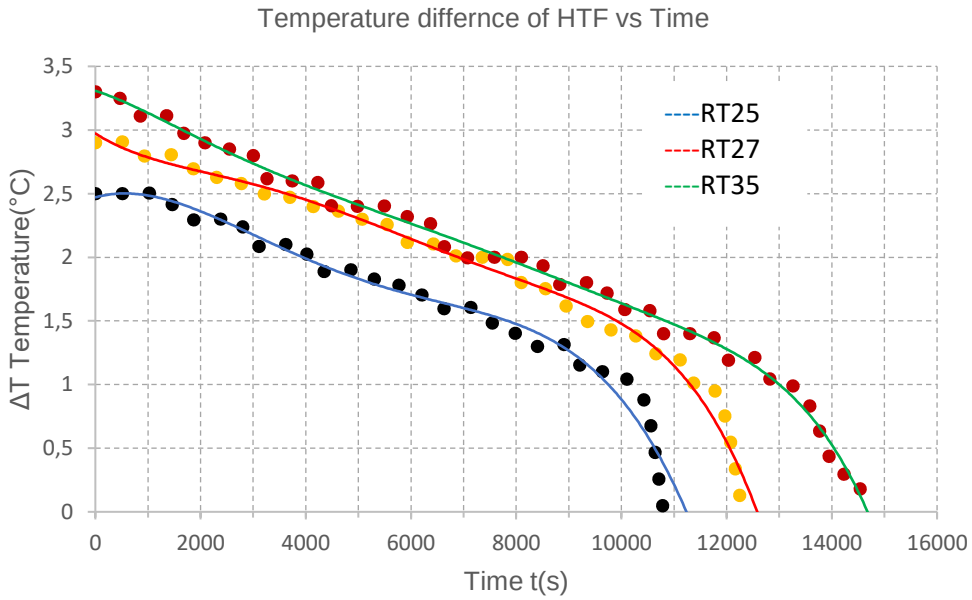

Figure 4.6: Discharging process–temperature difference of the water for each PCM at a flow rate of 600L/hr

Figure 4.6 shows the temperature difference vs. time of the water (flowing at a rate of 600 L/hr) as it recovered energy from each individual PCM. The time recorded for each PCM (RT25, RT27, and RT35) to complete the discharging period was 140, 150, and 160 minutes respectively.

Figures 4.4 to 4.6 also show the effect of varying the flow rates of the water during the discharging process of the PCM. An increase in the flow rate of the water has an inverse effect on the time that is required to discharge the energy from the PCM. As the water flow rate increases, the time required for the complete discharging becomes smaller. Table 4.2 shows the time required to discharge the stored thermal energy on the chosen PCMs at different flow rates and constant initial temperature of the HTF (water).

Table 4.2: Time to discharge stored thermal energy at different flow rates and constant initial inlet temperature of the HTF (water)

	Time to complete the discharging process		
	@ 200L/hr	**@ 400L/hr**	**@ 600L/hr**
HTF inlet temperature	**18 °C**	**18 °C**	**18 °C**
RT25 Time (minutes)	240	200	180
RT27 Time (minutes)	270	230	205
RT35 Time (minutes)	300	265	245

4.4 The amount of stored and recovered energy, in and from the PCM

The data recorded during the experiments when the charging and discharging processes were conducted were further utilised in calculating the total energy stored and recovered from the PCM respectively. That was achieved by the use of Equations 4.1 and 4.2 presented in Sections 4.2.1 and 4.2.2 respectively.

4.4.1 The effect of the flow rate of water on the energy stored in the PCM

Figure 4.7 displays the cumulative effect that the flow rate of the water had on each PCM's amount of energy stored during the charging process. Table 4.3, displaying the amount of energy stored in each PCM for each water flow rate and the time that it took for the completion of the process, is provided for the reader's ease/convenience when comparing the results. For each PCM, as the flow rate increased, the amount of total energy stored also increased. For example, for the RT25, the amounts of stored energy at the end of the charging processes were 6679 kJ in 180 minutes, 12141 kJ in 160 minutes, and 16698 kJ in 140 minutes respectively for the flow rates of water of 200, 400, and 600 L/hr respectively. In comparison with RT27, the stored energy after each process was 7225 kJ in 195 minutes, 13786 kJ in 175 minutes, and 21430 kJ in 150 minutes for the same flow rate range.

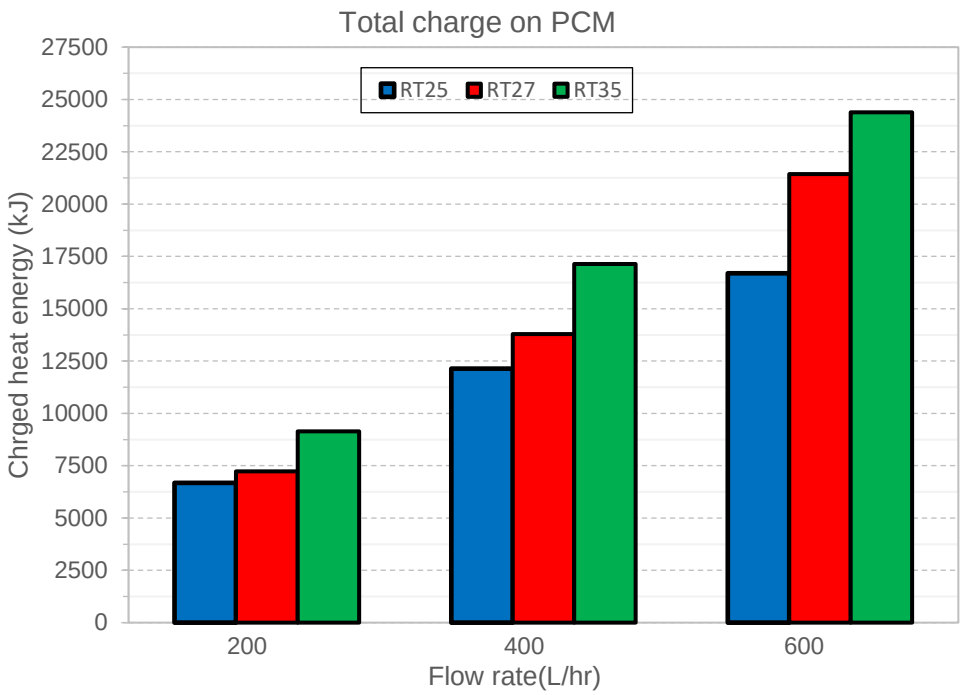

Figure 4.7: Comparison of energy stored in RT25, RT27 and RT35 after the charging process

The values of accumulated heat energy (Q_1) released by the hot water (70 °C) and stored on the PCMs located inside the storage tank, together with the time for the completion of the charging process for the three water flow rates, are shown in Table 4.3.

Table 4.3: Heat stored (Q_1) on the PCM during the charging time at different flow rates of the water

PCM		Flow rate of the hot water (70 °C)		
		200L/hr	400L/hr	600L/hr
RT25	Q_1 (kJ)	6679	12141	16698
	Time (min)	180	160	140
RT27	Q_1 (kJ)	7225	13786	21430
	Time (min)	195	175	150
RT35	Q_1 (kJ)	9145	17139	24390
	Time (min)	205	180	160

4.4.2 The effect of the flow rate of water on the energy released by the PCM

Figure 4.8 displays the cumulative effect that the flow rate of the water had on each PCM's amount of energy released during the discharging process. Table 4.4, displaying the amount of energy released by each PCM to the cold water for each water flow rate and the time that it took for the completion of the process, is provided for the reader's ease/convenience as explained in Section 4.4.1 above. For each PCM, as the flow rate increased, the amount of total energy released also increased. For example, for the RT25, the amounts of released energy at the end of the discharging processes were 4911 kJ in 240 minutes, 9130 kJ in 270 minutes, and 13592 kJ in 300 minutes for the flow rates of water at 200, 400, and 600 L/hr respectively.

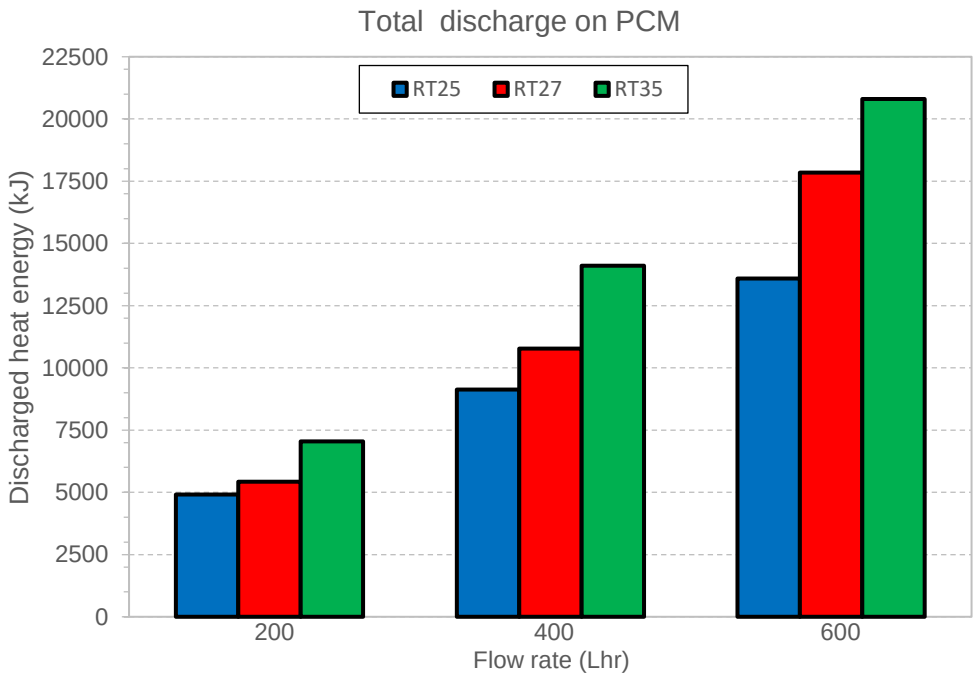

Figure 4.8:Comparison of energy released by RT25, RT27 and RT35 after the discharging process

The values of accumulated heat energy (Q_2) released by the PCMs located inside the storage tank to the cold water (18°C), together with the time for the completion of the discharging process for the three water flow rates, are shown in Table 4.4.

Table 4.4: Heat released by the PCM during the discharging time at different flow rates of the water

PCM		Flow rate of the cold water (18 °C)		
		200L/hr	400L/hr	600L/hr
RT25	Q_2(kJ)	4911	9130	13592
	Time (min)	240	200	180
RT27	Q_2(kJ)	5429	10775	17840
	Time (min)	270	230	205
RT35	Q_2(kJ)	7045	14100	20805
	Time (min)	300	265	245

4.4.3 On the thermal efficiency of the thermal storage unit relating to the chosen PCMs

The efficiency of the thermal energy storage system, in terms of the PCM used, is defined here as the ratio of the energy output from the thermal storage unit to the energy stored in it. The following expression has been adopted to compute the efficiency of the thermal energy storage used in the experiments in order to relate to the three chosen PCMs for the study:

$$\eta = Q_2/Q_1 \qquad (4.3)$$

where η is the efficiency, Q_1 and Q_2 represent the thermal energy charged/stored in and discharged from the PCM respectively.

Table 4.5 may be interpreted as the summary of the results pertaining to the behaviour of the three PCMs chosen for this study as they were subjected to the charging and discharging of thermal energy processes. Table 4.5 is, in fact, an extension of combining Tables 4.3 and 4.4, thus listing the amount of thermal energy that was stored (Q_1) as well as the amount that could be extracted (Q_2) to and from each PCM. Hence, efficiency could be attributed to them depending on the parameters of the process such as time, the flow rate, and temperatures of the HTF.

Table 4.5:Thermal efficiency of PCMs associated with their storage capacity

PCM		Flow rate of the hot water (70 °C) Flow rate of the cold water (18 °C)		
		200L/hr	400L/hr	600L/hr
RT25	Q_1(kJ)	6679	12141	16698
	Time (min)	180	160	140
	Q_2 (kJ)	4911	9130	13592
	Time (min)	240	200	180
	η	73%	75%	81%
RT27	Q_1(kJ)	7225	13786	21430
	Time (min)	195	175	150
	Q_2 (kJ)	5429	10775	17840
	Time (min)	270	230	205
	η	75%	78%	83%
RT35	Q_1(kJ)	9145	17139	24390
	Time (min)	205	180	160
	Q_2 (kJ)	7045	14100	20805
	Time (min)	300	265	245
	η	77%	82%	85%

4.5 Summary of the results and conclusions

The experimental investigation evaluated the performance of a helical coil latent heat energy storage unit, where the three chosen paraffin waxes (PCMs) were individually used during their phase change. The phase change of the material from solid to liquid took place during the charging process or while storing thermal energy on the PCM. The phase change from liquid to solid took place during the discharging process or thermal energy recovery from the PCM. The charging and discharging of thermal energy on each PCM were performed using three different flow rates for the HTF (common to all three). The inlet temperature of the (hot) HTF for the thermal charging process and similarly the (cold) inlet temperature of the HTF for the discharging process were also identical for all three PCMs. The following conclusions (when one observes/examines the information in Table 4.5) are drawn from the results of the experiments:

- During the charging process an increase in the flow rate of the HTF resulted in diminished time to complete the process for each PCM. This is in accordance with two facts:

1) The energy-carrying fluid moving faster brings energy more quickly to the material.
2) In the mechanism of heat transfer known as forced convection, the increase of velocity of a fluid in contact with a surface (the HTF flowing inside the helical tube) enhances the heat transfer coefficient between them and allows more heat to be transferred.

- The same effect on the time to complete the discharging process was observed when the flow rate of the HTF was increased. That is, the process ended more quickly because:

1) The cold HTF moving faster would take the energy away from the PCM more quickly.
2) Identical explanation of the behaviour of the heat transfer coefficient applies to this process as well.

- The effect of the flow rate of the HTF (for both charging and discharging modes) on the amount of thermal energy stored and recovered was identical. That is, the stored energy (Q_1) and recovered energy (Q_2) were both increased for the following reasons:

1) Increasing the flow rate of the HTF results in more fluid-quantity-carrying thermal energy for storing it or available to recover it from the PCM respectively.
2) As outlined before, increased fluid velocity increases the forced convection heat transfer coefficient, subsequently increasing the quantity of heat transferred between the fluid flowing and the internal surface of the helical pipe heat exchanger.

- The effect of an increase in the flow rate of the HTF was that it also increased the thermal efficiency (**η)** of the PCM; however, that was not necessarily expected since it is the ratio of Q_2 to Q_1. It possibly points to another factor: It was assumed that energy losses from the thermal storage unit to the environment could be ignored since they could be constant for all (identical) tests performed; however, the time factor was not foreseen. The longer it took for the process to be completed, the longer the storage

testing unit was exposed to losses to the environment, which would affect the thermal efficiency (**η)** of the PCM.

- Finally, in examining the results listed in Table 4.5, the PCM RT35 appears to have outperformed the other two PCMs because of high storage density and latent heat of melting of a phase change material, as well as high rate of heat absorption. It has better capabilities to release heat to the surroundings and also exhibits no phase segregation and super-cooling.
- Thermal energy storage is dependent upon the latent heat of melting of a phase change material, while energy discharge is dependent upon the rate at which solidification of the PCM takes place.

CHAPTER FIVE
CONCLUSIONS AND RECOMMENDATION

5.1 Conclusions

The aims of this study were to investigate or rank the capabilities of three PCMs to store thermal solar energy and release it when required. This could extend thermal comfort to households through renewable energy beyond the hours of sunshine.

Guided by a literature survey, the development of a latent heat thermal energy storage system, using phase change materials of the paraffin wax type, was accomplished. For the present study, the PCMs were selected based on the following criteria: large latent heat, high volumetric energy storage density, low volume changes with phase transition, low melting point within the practical range of operation, congruent melting with minimum super-cooling, no phase segregation, and good heat absorption characteristics as detailed in Chapter 3. Various tests emerging from the results were presented in Chapter 4, and it is concluded that:

The PCM RT35 appears to have outperformed the other two PCMs and could be selected as a suitable material for a thermal storage unit in space heating and cooling systems in order to improve their thermal efficiency and possibly reduce the peak heating and cooling electrical load.

Using water as the HTF in the system resulted in a low outlet temperature of the HTF which did not allow reasonable use of its energy in space heating. Air must be used instead of water as the HTF, which will allow a high enough exit temperature from the heat storage unit to be utilised for space heating.

A solar-powered space heating system could operate in three ways. When there is sunshine during the day and when we at any time need to use heat from the sun, enough air needs to pass through the solar collector and a mechanism into the home. In case we don’t need heat, air needs to be pumped into a special thermal storage device, melting the PCM, charging it for later use. When sunlight is unavailable, the air from the room could

be channelled through the thermal storage device, heated, and then distributed throughout the house. When the heat storage unit is solidified or the stored heat is depleted, an auxiliary gas heater system could be used to supply heat into the household (Belusko et al., 2004).

5.2 Recommendations for future work

Thermal energy storage applications using phase change materials need further investigation. For example, the optimisation of a helical coil heat exchanger to store harvested solar heat energy so that it may be used for home space heating and cooling using air as the heat transfer fluid could be explored.

REFERENCES

Abhat, A. 1981. Low temperature latent heat thermal energy storage: heat storage materials. *Solar Energy,* 30(4), pp. 313-331. https://doi.org/10.1016/0038-092X(83)90186-X

Adeyanju, A. & Manohar, K. 2009. Theoretical and experimental investigation of heat transfer in packed beds. *Research Journal of Applied Sciences*, 4(5), pp. 166-177.

Akgün, M., Aydın, O. & Kaygusuz, K. 2007. Experimental study on melting/solidification characteristics of a paraffin as PCM. *Energy Conversion and Management,* 48(2), pp. 669-678. https://doi.org/10.1016/j.enconman.2006.05.014

Alexiades, V. & Solomon, A.D. 1993. *Mathematical modeling of melting and freezing processes.* Washington, DC: Hemisphere.

Alkilani, M.M., Sopian, K., Mat., S. & Alghoul, M.A. 2009. Output air temperature prediction in a solar air heater integrated with phase change material. *European Journal of Scientific Research*, 27(3), pp. 334-341.

Amori, K.E. & Sherza, J.S. 2013. An investigation of shell-helical coiled tube heat exchanger used for solar water heating system. *Innovative Systems Design and Engineering,* 4(15), pp. 78-90.

Belusko, M., Saman, W. & Bruno, F. 2004. Roof integrated solar heating system with glazed collector. *Solar Energy*, 76(1-3), pp. 61-69. https://doi.org/10.1016/j.solener.2003.08.020

De Gracia, A. & Luisa, F., 2015. Phase change materials and thermal energy storage for buildings. *Energy buildings*, June, pp. 88.

Delaunay, D. & Carré, P. 1982. Dispositif de mesure automatique de la conductivité thermique des matériaux à changement de phase. *Revue de Physique Appliquée (Paris)*, 17(4), pp. 209-215.
https://doi.org/10.1051/rphysap:01982001704020900

Dinçer, I. & Rosen, M. 2002. *Thermal energy storage: systems and applications.* New York, NY: John Wiley.

Dinçer, I. & Rosen, M. 2010. *Thermal energy storage and energy savings.* 2nd ed. Hoboken, NJ: John Wiley.

Duffie, J.A. & Beckman, W.A. 2006. *Solar engineering of thermal processes.* 3rd ed. Hoboken, NJ: John Wiley.

Fang, G.D., Dionysiou, D.D., Wang, Y., Al-Abed, S.R. & Zhou, D.M. 2012. Sulfate radical-based degradation of polychlorinated biphenyls: effects of chloride ion and reaction kinetics. *Journal of Hazardous Materials*, 227-228, pp. 394-401. https://doi.org/10.1016/j.jhazmat.2012.05.074

Farid, M., Khudhair, A. M., Razack, S. & Al-Hallaj, S. 2004. A review on phase change energy storage: materials and applications. *Energy Conversion and Management,* 45(9-10), pp. 1597-1615. https://doi.org/10.1016/j.enconman.2003.09.015

Flaherty B. 1971. Characterisation of waxes by differential scanning calorimetry. *Journal of Applied Chemistry and Biotechnology*, 21(5), pp. 144-148. https://doi.org/10.1002/jctb.5020210507

Fluri, T. 2009. Solar resource mapping in South Africa. 27 March. [PowerPoint presentation].

Gao, W., Lin, T., Liu, C. & Xia, C. 2007. An experiment study on the heat storage performances of polyacohols NPG, TAM, PE, and AMPD and their mixtures as solid-solid phase-change materials for solar energy applications. *International Journal of Green Energy,* 4(3), pp. 301-311. https://doi.org/10.1080/15435070701332112

Hed, G., Young, A.P. & Domany, E. 2004. Lack of ultrametricity in the low-temperature phase of 3D Ising spin glasses. *Physical Review Letters,* 92, Article 157201. https://doi.org/10.1103/PhysRevLett.92.157201

Joulin, A., Younsi, Z., Zalewski, L., Rousse, D.R. & Lassue, S. 2009. A numerical study of the melting of phase change material heated from a vertical wall of a rectangular enclosure. *International Journal of Computational Fluid Dynamics*, 23(7), pp. 553-566. https://doi.org/10.1080/10618560903203723

Kang, Y., Zhang, Y., Zhu, Y. & Jiang, Y. 1999. A simple model for heat transfer analysis of shell and tube with phase change material and its performance simulation. *Acta Energiae Solaris Sinica*, 20(1), pp. 20-25.

Lane, G.A. 1980. Low temperature heat storage with phase change materials. *International Journal of Ambient Energy,* 1(3), pp.155-168. https://doi.org/10.1080/01430750.1980.9675731

Lane, G.A. 1986. *Solar heat storage: latent heat material.* Boca Raton, FL: CRC Press.

Loan, S.,& Calin, S., 2018. A Comprehensive Review of Thermal Energy Storage. *Sustainability,* 191(10).

Marín, J.M., Zalba, B., Cabeza, L.F & Mehling, H. 2003. Determination of enthalpy–temperature curves of phase change materials with the temperature-history method: improvement to temperature dependent properties. *Measurement Science and Technology*, 14(2), pp. 2027-2175. https://doi.org/10.1088/0957-0233/14/2/305

Mehling, H. & Cabeza, L.F. 2008. *Heat and cold storage with PCM: an up to date introduction into basics and applications.* Berlin: Springer.

Mettawee, E.B.S. & Assassa, G.M.R. 2007. Thermal conductivity enhancement in a latent heat storage system. *Solar Energy,* 81(7), pp. 839-845. https://doi.org/10.1016/j.solener.2006.11.009

Rubitherm. 2019. PCR-RT Line. www.rubitherm.eu/en/index.php/productcategory/organische-pcm-rt [24 November 2020].

Saman, W. & Belusko, M. 1997. Roof integrated unglazed transpired solar air heater. In Lee, T. (ed.). *Solar 97: "Sustainable Energy": 35th Annual Conference of the Australian and New Zealand Solar Energy Society, Canberra, Australia 1–3 December: Proceedings.* Sydney: The Society, Paper 66.

Sarbu, I. & Dorca, A. 2018. Review on heat transfer analysis in thermal energy storage using latent heat storage systems and phase change materials. *International Journal of Energy Research,* 43(1), pp. 29-64. https://doi.org/10.1002/er.4196

Sari, A. & Kaygusuz, K. 2006. Thermal energy storage characteristics of myristic and stearic acids eutectic mixture for low temperature heating applications. *Chinese Journal of Chemical Engineering*, 14(2), pp. 270-275. https://doi.org/10.1016/S1004-9541(06)60070-0

Satyanarayana, K., Sukumaran, K., Kulkarni, A.G., Pillai, S.G.K. & Rohatgi, P.K. 1986. Fabrication and properties of natural fibre-reinforced polyester composites. *Composites*, 17(4), pp. 329-333. https://doi.org/10.1016/0010-4361(86)90750-0

Shamsundar, N., Stein, E., Rooz, E., Bascaran, E. & Lee, T.C. 1992. Design and simulation of latent heat storage units. Final report. National Renewable Energy Laboratory, Golden, CO.

Sharma, A. & Chen, C. 2009. Solar water heating system with phase change materials. *International Review of Chemical Engineering*, 1, pp. 297-307.

Sharma, A., Tyagi, V.V., Chen, C.R. & Buddhi, D. 2009. Review on thermal energy storage with phase change materials and applications. *Renewable and Sustainable Energy Reviews*, 13(2), pp. 318–345. https://doi.org/10.1016/j.rser.2007.10.005

Sharma, S.D., Iwata, T., Kitano, H. & Sagara, K. 2005. Thermal performance of a solar cooker based on an evacuated tube solar collector with a PCM storage unit. *Solar Energy*, 78(3), pp. 416-426.

Speyer, R.F. 1994. *Thermal analysis of materials.* 5th ed. New York, NY: Marcel Dekker.

Syed, A.M. & Hachem, C. 2019. Review of design trends in lighting, environmental controls, carbon dioxide supplementation, passive design, and renewable energy systems for agricultural greenhouses. *Journal of Biosystems Engineering*, 44(1), pp. 28-36. https://doi.org/10.1007/s42853-019-00006-0

Takeda, S., Nagano, K., Mochida, T. & Shimakura, K. 2004. Development of a ventilation system utilizing thermal energy storage for granules containing phase change material. *Solar Energy*, 77(3), pp. 329-338. https://doi.org/10.1016/j.solener.2004.04.014

Thakare, A.M. & Deshmukh, S.J. 2018. Performance analysis of solar powered adsorption cooling system. Paper presented at the 2018 International Conference and Utility Exhibition on Green Energy for Sustainable Development (ICUE), Phuket, Thailand, 24–26 October, 5 pp. doi: 10.23919/ICUE-GESD.2018.8635690

Wang, J., Ouyang, Y. & Chen, G. 2001. Experimental study on charging processes of a cylindrical heat storage capsule employing multiple phase change materials. *International Journal of Energy Research,* 25(5), pp. 439-447. https://doi.org/10.1002/er.695

Winkler, H. 2004. Renewable energy policy in South Africa: policy options for renewable electricity. *Energy Policy,* 33, pp. 27-38.

Yang, X., Lu, Z., Bai, Q., Zhang, Q., Jin, L. & Yan, J. 2017. Thermal performance of a shell-and-tube latent heat thermal energy storage unit: role of annular fins. *Applied Energy*, 202, pp. 558-570.

Yang, Z.,Chen, L., Li, Y., Xia, Z. & Wang, C. 2019. Numerical investigation of heat transfer characteristics in a shell-and-tube latent heat thermal energy storage system. *Energy Procedia*, 160, pp. 475-482. https://doi.org/10.1016/j.egypro.2019.02.195

Zalba, B., Marín, J.M., Cabeza, L.F. & Mehling, H. 2003. Review on thermal energy storage with phase change: materials, heat transfer analysis and applications. *Applied Thermal Engineering,* 23(3), pp. 251-283. https://doi.org/10.1016/S1359-4311(02)00192-8

Zhu, Y., Zhang, Y., Jiang, Y. & Kang, Y. 1999. Thermal storage and heat transfer in phase change material outside a circular tube with axial variation of the heat transfer fluid temperature. *Journal of Solar Energy Engineering,* 121(3), pp. 145-149. https://doi.org/10.1115/1.2888425

APPENDICES

APPENDIX A: Rubitherm Phase Change Materials before and after solidification

Appendix A compares the Rubithem RT PCMs' behaviour after usage. In Figure A-1 the RT category is shown as it appears before it is tested for thermal energy storage behaviour. Figure A-2 depicts how the RT PCMs solidify after absorbing, then releasing energy.

Figure 0.1: Phase change materials based on n-paraffins and waxes (Rubertherm, 2019)

Figure 0.2: Solidified RT category PCM

APPENDIX B: PCM Secondary data (supplied by Rubitherm)

Appendix B provides Rubitherm data of RT category of PCMs that are organic materials. Properties of the three types of RT considered in this work, including RT25, RT27 and RT35, are given respectively in Tables B-1, B-2 and B-3.

Table 0.1: Rubitherm RT25 properties

Property	Unit	Typical Values
Melting point (approx.)	°C	25
Congealing point (PCM)	°C	24
Heat storage capacity *Temperature -3°C* to *12°C*	kJ/(kg)	179
Density solid *at 15°C*	kg/m^3	0.87
Density liquid *At 15°C I 70°C*	kg/m^3	0.75
Volume expansion	%	10
Volume expansion *without phase change*	K^{-1}	0.001
Specific heat capacity	kJ/(kg.K)	1.8/2.4
Thermal conductivity	W/(mK)	0.2
Kinetic viscosity @ 40 °C	m^2/s	4.5
Flash point (PCM)	°C	164
Corrosion		Chemically inert
Water hazard		Water hazard class (WGK)1

Table 0.2: Rubitherm RT27 properties

Property	Unit	Typical Values
Melting point (approx.)	°C	28
Congealing point (PCM)	°C	26
Heat storage capacity *Temperature -3°C to 12°C*	kJ/(kg)	179
Density solid *at 15°C*	kg/m^3	0.87
Density liquid *At 15°C I 70°C*	kg/m^3	0.75
Volume expansion	%	10
Volume expansion *without phase change*	K^{-1}	0.001
Specific heat capacity	kJ/(kg.K)	1.8/2.4
Thermal conductivity	W/(mK)	0.2
Kinetic viscosity @ 40°C	m^2/s	4.5
Flash point (PCM)	°C	164
Corrosion		Chemically inert
Water hazard		Water hazard class (WGK)1

Table 0.3: Rubitherm RT27 properties

Property	Unit	Typical Values
Melting point (approx.)	*°C*	35
Congealing point (PCM)	*°C*	36
Heat storage capacity *Temperature -3°C* to *12°C*	kJ/(kg)	157
Density solid *at 15°C*	kg/m^3	0.88
Density liquid *At 15°C I 70°C*	kg/m^3	0.76
Volume expansion	%	10
Volume expansion *without phase change*	K^{-1}	0.001
Specific heat capacity	kJ/(kg.K)	1.8/2.4
Thermal conductivity	W/(mK)	0.2
Kinetic viscosity @ 40*°C*	m^2/s	3.3
Flash point (PCM)	*°C*	178
Corrosion		Chemically inert
Water hazard		No water endangering substance

APPENDIX C: Heat exchanger specifications

Table 0.4: **Technical specifications of the heat exchanger**

Type	Shell & Tube
Shell diameter	30 cm
Length	200 cm
Shell thickness	0.4 cm
Pitch circle diameter	10 cm
Number of turns in helical coil, N	10
tube outside diameter d (mm)	0.8 cm
tube inside diameter di (mm)	2 cm
Tube thickness	0.2 cm
Axial length of helical coil (m)	4 Longitudinal
Coil diameter, tube-centre-to-tube centre Dc (mm)	1.0 cm
Coil pitch p (mm)	0.1 cm
Curvature ratio, di/ Dc	
Capacity of shell	30kg
Material	Stainless steel

APPENDIX D: Sample of collected data

Appendix D provides samples of collected data for both charging and discharging phases during the experiment using RT25, RT27 and RT35. Tables D1 to D9 show the charging, while Tables D10 to D18 give the discharging phase.

Table 0.1:Results of RT25 during the charging phase with a flow rate of 200L/hr

Time (sec)	T_2 (°C)	T_1 (°C)	ΔT(°C)	Cp_w(J/kg°C)	Mass flow rate(kg/sec)	Q_1(kJ)
0	70	66.0	4.0	4186	0.055	**2.8E+02**
300	70	66.0	4.0	4186	0.055	**2.8E+02**
600	70	66.0	4.0	4186	0.055	**2.7E+02**
900	70	66.1	3.9	4186	0.055	**2.7E+02**
1200	70	66.1	3.9	4186	0.055	**2.7E+02**
1500	70	66.1	3.9	4186	0.055	**2.7E+02**
1800	70	66.2	3.8	4186	0.055	**2.6E+02**
2100	70	66.2	3.8	4186	0.055	**2.6E+02**
2400	70	66.2	3.8	4186	0.055	**2.6E+02**
2700	70	66.4	3.6	4186	0.055	**2.5E+02**
3000	70	66.4	3.6	4186	0.055	**2.4E+02**
3300	70	66.6	3.4	4186	0.055	**2.3E+02**
3600	70	66.6	3.4	4186	0.055	**2.3E+02**
3900	70	66.6	3.4	4186	0.055	**2.3E+02**
4200	70	66.7	3.3	4186	0.055	**2.3E+02**
4500	70	66.7	3.3	4186	0.055	**2.2E+02**
4800	70	66.9	3.1	4186	0.055	**2.1E+02**
5100	70	66.9	3.1	4186	0.055	**2.1E+02**
5400	70	67.1	2.9	4186	0.055	**1.9E+02**
5700	70	67.5	2.5	4186	0.055	**1.7E+02**
6000	70	67.6	2.4	4186	0.055	**1.6E+02**
6300	70	67.7	2.3	4186	0.055	**1.6E+02**
6600	70	67.7	2.3	4186	0.055	**1.5E+02**
6900	70	67.9	2.1	4186	0.055	**1.5E+02**
7200	70	67.9	2.1	4186	0.055	**1.5E+02**
7500	70	67.9	2.1	4186	0.055	**1.4E+02**
7800	70	68.0	2.0	4186	0.055	**1.3E+02**
8100	70	68.1	1.9	4186	0.055	**1.3E+02**

8400	70	68.2	1.8	4186	0.055	**1.1E+02**
8700	70	68.7	1.3	4186	0.055	**9.0E+01**
9000	70	68.7	1.3	4186	0.055	**8.6E+01**
9300	70	68.8	1.2	4186	0.055	**7.9E+01**
9600	70	68.9	1.1	4186	0.055	**6.9E+01**
9900	70	69.1	0.9	4186	0.055	**5.5E+01**
10200	70	69.3	0.7	4186	0.055	**4.1E+01**
10500	70	69.5	0.5	4186	0.055	**1.7E+01**
10800	70	70.0	0.0	4186	0.055	**0.0E+00**

Table 0.2: Results of RT25 during the charging phase with a flow rate of 400L/hr

Time(sec)	T_2 (°C)	T_1 (°C)	ΔT(°C)	Cp_w(J/kg°C)	Mass flow rate(kg/sec)	Q_1(kJ)
0	70	70	4.1	4186	0.112	**571.5**
300	70	69.4	4.1	4186	0.112	**5.72E+02**
600	70	69.4	4.1	4186	0.112	**5.72E+02**
900	70	69.3	4.0	4186	0.112	**5.58E+02**
1200	70	69.3	4.0	4186	0.112	**5.58E+02**
1500	70	69.2	3.6	4186	0.112	**5.02E+02**
1800	70	69.2	3.6	4186	0.112	**5.02E+02**
2100	70	69.1	3.5	4186	0.112	**4.88E+02**
2400	70	69.1	3.5	4186	0.112	**4.88E+02**
2700	70	69.1	3.5	4186	0.112	**4.88E+02**
3000	70	69.1	3.4	4186	0.112	**4.74E+02**
3300	70	69	3.3	4186	0.112	**4.60E+02**
3600	70	69	3.3	4186	0.112	**4.60E+02**
3900	70	69	3.2	4186	0.112	**4.46E+02**
4200	70	68.8	3.2	4186	0.112	**4.46E+02**
4500	70	68.8	3.2	4186	0.112	**4.46E+02**
4800	70	68.8	3.0	4186	0.112	**4.18E+02**
5100	70	68.8	2.8	4186	0.112	**3.90E+02**
5400	70	68.7	2.5	4186	0.112	**3.48E+02**
5700	70	68.7	2.5	4186	0.112	**3.48E+02**
6000	70	68.7	2.3	4186	0.112	**3.21E+02**
6300	70	68.6	2.3	4186	0.112	**3.21E+02**
6600	70	68.6	2.1	4186	0.112	**2.93E+02**

6900	70	68.6	2.1	4186	0.112	**2.93E+02**
7200	70	68.6	1.8	4186	0.112	**2.51E+02**
7500	70	68.6	1.8	4186	0.112	**2.51E+02**
7800	70	68.5	1.5	4186	0.112	**2.09E+02**
8100	70	68.5	1.5	4186	0.112	**2.09E+02**
8400	70	68.5	1.2	4186	0.112	**1.67E+02**
8700	70	68.5	1.2	4186	0.112	**1.67E+02**
9000	70	68.4	0.5	4186	0.112	**6.97E+01**
9300	70	68.4	0.4	4186	0.112	**5.58E+01**
9600	70	70	0.0	4186	0.112	**0.00E+00**

Table 0.3: Results of RT25 during the charging phase with a flow rate of 600L/hr

Time(sec)	T_2 (°C)	T_1 (°C)	ΔT(°C)	Cp_w(J/kg°C)	Mass flow rate(kg/sec)	Q_1(kJ)
0	70	66.0	4.0	4186	0.168	**833.9**
300	70	69	4.0	4186	0.168	**8.34E+02**
600	70	69	4.0	4186	0.168	**8.34E+02**
900	70	69	4.0	4186	0.168	**8.34E+02**
1200	70	69	4.0	4186	0.168	**8.34E+02**
1500	70	69	3.7	4186	0.168	**7.71E+02**
1800	70	68.9	3.7	4186	0.168	**7.71E+02**
2100	70	68.7	3.7	4186	0.168	**7.71E+02**
2400	70	68.8	3.7	4186	0.168	**7.71E+02**
2700	70	68.7	3.5	4186	0.168	**7.30E+02**
3000	70	68.7	3.5	4186	0.168	**7.30E+02**
3300	70	68.7	3.5	4186	0.168	**7.30E+02**
3600	70	68.7	3.2	4186	0.168	**6.67E+02**
3900	70	68.6	3.0	4186	0.168	**6.25E+02**
4200	70	68.6	3.0	4186	0.168	**6.25E+02**
4500	70	68.6	2.8	4186	0.168	**5.84E+02**
4800	70	68.6	2.8	4186	0.168	**5.84E+02**
5100	70	68.5	2.5	4186	0.168	**5.21E+02**
5400	70	68.5	2.3	4186	0.168	**4.79E+02**
5700	70	68.5	2.2	4186	0.168	**4.59E+02**
6000	70	68.5	2.1	4186	0.168	**4.38E+02**
6300	70	68.5	2.0	4186	0.168	**4.17E+02**

6600	70	68.5	2.0	4186	0.168	**4.17E+02**
6900	70	68.3	1.9	4186	0.168	**3.96E+02**
7200	70	68.3	1.7	4186	0.168	**3.54E+02**
7500	70	68.3	1.5	4186	0.168	**3.13E+02**
7800	70	68.3	1.3	4186	0.168	**2.71E+02**
8100	70	68.3	0.5	4186	0.168	**1.04E+02**
8400	70	70	0.0	4186	0.168	**0.00E+00**

Table 0.4: Results of RT27 during the charging phase with a flow rate of 200L/hr

Time(sec)	T_2 (°C)	T_1 (°C)	ΔT(°C)	Cp_w(J/kg°C)	Mass flow rate(kg/sec)	Q_1(kJ)
300	70	65.8	4.2	4186	0.056	**2.95E+02**
600	70	65.8	4.2	4186	0.056	**2.88E+02**
900	70	65.9	4.1	4186	0.056	**2.81E+02**
1200	70	66.0	4.0	4186	0.056	**2.81E+02**
1500	70	66.0	4.0	4186	0.056	**2.81E+02**
1800	70	66.0	4.0	4186	0.056	**2.81E+02**
2100	70	66.0	4.0	4186	0.056	**2.74E+02**
2400	70	66.1	3.9	4186	0.056	**2.67E+02**
2700	70	66.2	3.8	4186	0.056	**2.67E+02**
3000	70	66.2	3.8	4186	0.056	**2.60E+02**
3300	70	66.3	3.7	4186	0.056	**2.60E+02**
3600	70	66.3	3.7	4186	0.056	**2.46E+02**
3900	70	66.5	3.5	4186	0.056	**2.39E+02**
4200	70	66.6	3.4	4186	0.056	**2.32E+02**
4500	70	66.7	3.3	4186	0.056	**2.18E+02**
4800	70	66.9	3.1	4186	0.056	**2.18E+02**
5100	70	66.9	3.1	4186	0.056	**2.18E+02**
5400	70	66.9	3.1	4186	0.056	**2.11E+02**
5700	70	67.0	3.0	4186	0.056	**1.97E+02**
6000	70	67.2	2.8	4186	0.056	**1.83E+02**
6300	70	67.4	2.6	4186	0.056	**1.83E+02**
6600	70	67.4	2.6	4186	0.056	**1.76E+02**
6900	70	67.5	2.5	4186	0.056	**1.76E+02**
7200	70	67.5	2.5	4186	0.056	**1.69E+02**
7500	70	67.6	2.4	4186	0.056	**1.62E+02**
7800	70	67.7	2.3	4186	0.056	**1.55E+02**
8100	70	67.8	2.2	4186	0.056	**1.48E+02**
8400	70	67.9	2.1	4186	0.056	**1.34E+02**
8700	70	68.1	1.9	4186	0.056	**1.20E+02**

9000	70	68.3	1.7	4186	0.056	**1.05E+02**
9300	70	68.5	1.5	4186	0.056	**9.85E+01**
9600	70	68.6	1.4	4186	0.056	**9.85E+01**
9900	70	68.6	1.4	4186	0.056	**8.44E+01**
10200	70	68.8	1.2	4186	0.056	**7.74E+01**
10500	70	68.9	1.1	4186	0.056	**7.03E+01**
10800	70	69.0	1.0	4186	0.056	**4.92E+01**
11100	70	69.3	0.7	4186	0.056	**3.52E+01**
11400	70	69.5	0.5	4186	0.056	**2.11E+01**
11700	70	69.7	0.3	4186	0.056	**2.11E+01**
12000	70	70.0	0.0	4186	0.056	**0.00E+00**

Table 0.5: Results of RT27 during the charging phase with a flow rate of 400L/hr

Time(sec)	T_2 (°C)	T_1 (°C)	ΔT(°C)	Cp_w(J/kg°C)	Mass flow rate(kg/sec)	Q_1(kJ)
300	70	65.7	4.3	4186	0.112	**604.8**
600	70	65.7	4.3	4186	0.112	**604.8**
900	70	65.7	4.3	4186	0.112	**604.8**
1200	70	65.7	4.3	4186	0.112	**604.8**
1500	70	65.7	4.3	4186	0.112	**604.8**
1800	70	65.9	4.1	4186	0.112	**576.7**
2100	70	65.9	4.1	4186	0.112	**576.7**
2400	70	66.1	3.9	4186	0.112	**548.5**
2700	70	66.2	3.8	4186	0.112	**534.5**
3000	70	66.2	3.8	4186	0.112	**534.5**
3300	70	66.4	3.6	4186	0.112	**506.3**
3600	70	66.4	3.6	4186	0.112	**506.3**
3900	70	66.5	3.5	4186	0.112	**492.3**
4200	70	66.6	3.4	4186	0.112	**478.2**
4500	70	66.6	3.4	4186	0.112	**478.2**
4800	70	66.8	3.2	4186	0.112	**450.1**
5100	70	66.8	3.2	4186	0.112	**450.1**
5400	70	67.0	3.0	4186	0.112	**421.9**
5700	70	67.2	2.8	4186	0.112	**393.8**
6000	70	67.4	2.6	4186	0.112	**365.7**
6300	70	67.4	2.6	4186	0.112	**365.7**
6600	70	67.6	2.4	4186	0.112	**337.6**

6900	70	67.6	2.4	4186	0.112	**337.6**
7200	70	67.6	2.4	4186	0.112	**337.6**
7500	70	67.8	2.2	4186	0.112	**309.4**
7800	70	67.8	2.2	4186	0.112	**309.4**
8100	70	67.9	2.1	4186	0.112	**295.4**
8400	70	68.0	2.0	4186	0.112	**281.3**
8700	70	68.2	1.8	4186	0.112	**253.2**
9000	70	68.4	1.6	4186	0.112	**225.0**
9300	70	68.7	1.3	4186	0.112	**182.8**
9600	70	68.9	1.1	4186	0.112	**154.7**
9900	70	69.2	0.8	4186	0.112	**112.5**
10200	70	69.5	0.5	4186	0.112	**70.3**
10500	70	70.0	0.0	4186	0.112	**0.0**

Table 0.6: Results of RT27 during the charging phase with a flow rate of 600L/hr

Time(sec)	T_2 (°C)	T_1 (°C)	ΔT(°C)	Cp_w(J/kg°C)	Mass flow rate(kg/sec)	Q_1(kJ)
300	70.0	65.2	4.8	4186	0.168	**1012.7**
600	70.0	65.2	4.8	4186	0.168	**1012.7**
900	70.0	65.2	4.8	4186	0.168	**1012.7**
1200	70.0	65.2	4.8	4186	0.168	**1012.7**
1500	70.0	65.4	4.6	4186	0.168	**970.5**
1800	70.0	65.4	4.6	4186	0.168	**970.5**
2100	70.0	65.6	4.4	4186	0.168	**928.3**
2400	70.0	65.6	4.4	4186	0.168	**928.3**
2700	70.0	65.6	4.4	4186	0.168	**928.3**
3000	70.0	65.8	4.2	4186	0.168	**886.1**
3300	70.0	65.8	4.2	4186	0.168	**886.1**
3600	70.0	65.9	4.1	4186	0.168	**865.0**
3900	70.0	66.0	4.0	4186	0.168	**843.9**
4200	70.0	66.3	3.7	4186	0.168	**780.6**
4500	70.0	66.3	3.7	4186	0.168	**780.6**
4800	70.0	66.5	3.5	4186	0.168	**738.4**
5100	70.0	66.5	3.5	4186	0.168	**738.4**
5400	70.0	66.5	3.5	4186	0.168	**738.4**
5700	70.0	66.8	3.2	4186	0.168	**675.1**

6000	70.0	66.9	3.1	4186	0.168	**654.0**
6300	70.0	67.0	3.0	4186	0.168	**632.9**
6600	70.0	67.2	2.8	4186	0.168	**590.7**
6900	70.0	67.2	2.8	4186	0.168	**590.7**
7200	70.0	67.4	2.6	4186	0.168	**548.5**
7500	70.0	67.7	2.3	4186	0.168	**485.2**
7800	70.0	68.0	2.0	4186	0.168	**421.9**
8100	70.0	68.2	1.8	4186	0.168	**379.8**
8400	70.0	68.5	1.5	4186	0.168	**316.5**
8700	70.0	68.8	1.2	4186	0.168	**253.2**
9000	70.0	69.5	0.5	4186	0.168	**105.5**
9300	70.0	70.0	0.0	4186	0.168	**0.0**

Table 0.7: Results of RT35 during the charging phase with a flow rate of 200L/hr

Time(sec)	T_2 (°C)	T_1 (°C)	ΔT(°C)	Cp_w(J/kg°C)	Mass flow rate(kg/sec)	Q_1(kJ)
300	70.0	65.4	4.6	4186	0.056	**3.23E+02**
600	70.0	65.4	4.6	4186	0.056	**3.23E+02**
900	70.0	65.6	4.4	4186	0.056	**3.09E+02**
1200	70.0	65.6	4.4	4186	0.056	**3.09E+02**
1500	70.0	65.7	4.3	4186	0.056	**3.02E+02**
1800	70.0	65.8	4.2	4186	0.056	**2.95E+02**
2100	70.0	65.8	4.2	4186	0.056	**2.95E+02**
2400	70.0	65.8	4.2	4186	0.056	**2.95E+02**
2700	70.0	65.9	4.1	4186	0.056	**2.88E+02**
3000	70.0	65.9	4.1	4186	0.056	**2.88E+02**
3300	70.0	65.9	4.1	4186	0.056	**2.88E+02**
3600	70.0	65.9	4.1	4186	0.056	**2.88E+02**
3900	70.0	66.0	4.0	4186	0.056	**2.81E+02**
4200	70.0	66.0	4.0	4186	0.056	**2.81E+02**
4500	70.0	66.0	4.0	4186	0.056	**2.81E+02**
4800	70.0	66.0	4.0	4186	0.056	**2.81E+02**
5100	70.0	66.2	3.8	4186	0.056	**2.67E+02**
5400	70.0	66.2	3.8	4186	0.056	**2.67E+02**
5700	70.0	66.4	3.6	4186	0.056	**2.53E+02**
6000	70.0	66.4	3.6	4186	0.056	**2.53E+02**
6300	70.0	66.4	3.6	4186	0.056	**2.53E+02**
6600	70.0	66.6	3.4	4186	0.056	**2.39E+02**
6900	70.0	66.6	3.4	4186	0.056	**2.39E+02**

7200	70.0	66.6	3.4	4186	0.056	**2.39E+02**
7500	70.0	66.8	3.2	4186	0.056	**2.25E+02**
7800	70.0	66.8	3.2	4186	0.056	**2.25E+02**
8100	70.0	67.0	3.0	4186	0.056	**2.11E+02**
8400	70.0	67.0	3.0	4186	0.056	**2.11E+02**
8700	70.0	67.3	2.7	4186	0.056	**1.90E+02**
9000	70.0	67.3	2.7	4186	0.056	**1.90E+02**
9300	70.0	67.5	2.5	4186	0.056	**1.76E+02**
9600	70.0	67.7	2.3	4186	0.056	**1.62E+02**
9900	70.0	67.7	2.3	4186	0.056	**1.62E+02**
10200	70.0	67.9	2.1	4186	0.056	**1.48E+02**
10500	70.0	67.9	2.1	4186	0.056	**1.48E+02**
10800	70.0	68.1	1.9	4186	0.056	**1.34E+02**
11100	70.0	68.4	1.6	4186	0.056	**1.13E+02**
11400	70.0	68.7	1.3	4186	0.056	**9.14E+01**
11700	70.0	68.8	1.2	4186	0.056	**8.44E+01**
12000	70.0	69.1	0.9	4186	0.056	**6.33E+01**
12300	70.0	69.5	0.5	4186	0.056	**3.52E+01**
12600	70.0	70.0	0.0	4186	0.056	**0.00E+00**

Table 0.8: Results of RT35 during the charging phase with a flow rate of 400L/hr

Time(sec)	T_2 (°C)	T_1 (°C)	ΔT(°C)	Cp_w(J/kg°C)	Mass flow rate(kg/sec)	Q_1(kJ)
300	70.0	69.4	5.0	4186	0.112	**703.2**
600	70.0	69.4	5.0	4186	0.112	**703.2**
900	70.0	69.4	5.0	4186	0.112	**703.2**
1200	70.0	69.0	5.0	4186	0.112	**703.2**
1500	70.0	69.0	4.8	4186	0.112	**675.1**
1800	70.0	69.0	4.8	4186	0.112	**675.1**
2100	70.0	69.0	4.8	4186	0.112	**675.1**
2400	70.0	68.7	4.6	4186	0.112	**647.0**
2700	70.0	68.5	4.6	4186	0.112	**647.0**
3000	70.0	68.5	4.6	4186	0.112	**647.0**
3300	70.0	68.4	4.4	4186	0.112	**618.9**
3600	70.0	68.4	4.4	4186	0.112	**618.9**
3900	70.0	68.2	4.4	4186	0.112	**618.9**
4200	70.0	68.2	4.3	4186	0.112	**604.8**
4500	70.0	68.2	4.3	4186	0.112	**604.8**
4800	70.0	68.2	4.2	4186	0.112	**590.7**

5100	70.0	68.2	4.1	4186	0.112	**576.7**
5400	70.0	68.0	3.9	4186	0.112	**548.5**
5700	70.0	68.0	3.7	4186	0.112	**520.4**
6000	70.0	67.7	3.4	4186	0.112	**478.2**
6300	70.0	67.6	3.1	4186	0.112	**436.0**
6600	70.0	67.6	2.8	4186	0.112	**393.8**
6900	70.0	67.6	2.8	4186	0.112	**393.8**
7200	70.0	67.4	2.8	4186	0.112	**393.8**
7500	70.0	67.2	2.7	4186	0.112	**379.8**
7800	70.0	67.2	2.7	4186	0.112	**379.8**
8100	70.0	67.2	2.6	4186	0.112	**365.7**
8400	70.0	67.0	2.4	4186	0.112	**337.6**
8700	70.0	67.0	2.2	4186	0.112	**309.4**
9000	70.0	66.8	2.0	4186	0.112	**281.3**
9300	70.0	66.7	1.9	4186	0.112	**267.2**
9600	70.0	66.5	1.6	4186	0.112	**225.0**
9900	70.0	66.5	1.5	4186	0.112	**211.0**
10200	70.0	66.3	1.1	4186	0.112	**154.7**
10500	70.0	66.3	1.0	4186	0.112	**133.6**
10800	70.0	66.1	0.5	4186	0.112	**70.3**
11100	70.0	66.1	0.0	4186	0.112	**0.0**

Table 0.9: Results of RT35 during the charging phase with a flow rate of 600L/hr

Time(sec)	T_2 (°C)	T_1 (°C)	ΔT(°C)	Cp_w(J/kg°C)	Mass flow rate(kg/sec)	Q_1(kJ)
300	70.0	64.8	5.2	4186	0.168	**1097.1**
600	70.0	64.8	5.2	4186	0.168	**1097.1**
900	70.0	64.8	5.2	4186	0.168	**1097.1**
1200	70.0	65.0	5.0	4186	0.168	**1054.9**
1500	70.0	64.9	5.1	4186	0.168	**1076.0**
1800	70.0	65.1	4.9	4186	0.168	**1033.8**
2100	70.0	65.1	4.9	4186	0.168	**1033.8**
2400	70.0	65.1	4.9	4186	0.168	**1033.8**
2700	70.0	65.2	4.8	4186	0.168	**1012.7**
3000	70.0	65.4	4.6	4186	0.168	**970.5**
3300	70.0	65.4	4.6	4186	0.168	**970.5**
3600	70.0	65.6	4.4	4186	0.168	**928.3**

3900	70.0	65.6	4.4	4186	0.168	**928.3**
4200	70.0	65.8	4.2	4186	0.168	**886.1**
4500	70.0	66.0	4.0	4186	0.168	**843.9**
4800	70.0	66.0	4.0	4186	0.168	**843.9**
5100	70.0	66.1	3.9	4186	0.168	**822.8**
5400	70.0	66.1	3.9	4186	0.168	**822.8**
5700	70.0	66.3	3.7	4186	0.168	**780.6**
6000	70.0	66.3	3.7	4186	0.168	**780.6**
6300	70.0	66.5	3.5	4186	0.168	**738.4**
6600	70.0	66.7	3.3	4186	0.168	**696.2**
6900	70.0	66.9	3.1	4186	0.168	**654.0**
7200	70.0	67.0	3.0	4186	0.168	**632.9**
7500	70.0	67.2	2.8	4186	0.168	**590.7**
7800	70.0	67.5	2.5	4186	0.168	**527.4**
8100	70.0	67.9	2.1	4186	0.168	**443.0**
8400	70.0	68.2	1.8	4186	0.168	**379.8**
8700	70.0	68.4	1.6	4186	0.168	**337.6**
9000	70.0	68.6	1.4	4186	0.168	**295.4**
9300	70.0	69.2	0.8	4186	0.168	**168.8**
9600	70.0	69.5	0.5	4186	0.168	**105.5**
9900	70.0	70.0	0.0	4186	0.168	**0.0**

Table 0.10: Results of RT25 during the discharging phase with a flow rate of 200L/hr

Time(sec)	T_3(°C)	T_4 (°C)	ΔT(°C)	Cp_w(J/kg°C)	Mass flow rate(kg/sec)	Q_2(kJ)
0	18	20.3	2.3	4186	0.056	**1.6E+02**
300	18	20.3	2.3	4186	0.056	**1.6E+02**
600	18	20.3	2.3	4186	0.056	**1.6E+02**
900	18	20.2	2.2	4186	0.056	**1.5E+02**
1200	18	20.2	2.2	4186	0.056	**1.5E+02**
1500	18	20.2	2.2	4186	0.056	**1.5E+02**
1800	18	20.1	2.1	4186	0.056	**1.5E+02**
2100	18	20.1	2.1	4186	0.056	**1.5E+02**
2400	18	20.1	2.1	4186	0.056	**1.5E+02**
2700	18	20.0	2.0	4186	0.056	**1.4E+02**
3000	18	20.0	2.0	4186	0.056	**1.4E+02**
3300	18	20.0	2.0	4186	0.056	**1.4E+02**
3600	18	20.0	2.0	4186	0.056	**1.4E+02**
3900	18	20.0	2.0	4186	0.056	**1.4E+02**
4200	18	20.0	2.0	4186	0.056	**1.4E+02**
4500	18	20.0	2.0	4186	0.056	**1.4E+02**
4800	18	20.0	2.0	4186	0.056	**1.4E+02**
5100	18	19.9	1.9	4186	0.056	**1.3E+02**
5400	18	19.9	1.9	4186	0.056	**1.3E+02**
5700	18	19.7	1.7	4186	0.056	**1.2E+02**
6000	18	19.7	1.7	4186	0.056	**1.2E+02**
6300	18	19.7	1.7	4186	0.056	**1.2E+02**
6600	18	19.6	1.6	4186	0.056	**1.1E+02**
6900	18	19.6	1.6	4186	0.056	**1.1E+02**
7200	18	19.4	1.4	4186	0.056	**9.8E+01**
7500	18	19.4	1.4	4186	0.056	**9.8E+01**
7800	18	19.4	1.4	4186	0.056	**9.8E+01**
8100	18	19.4	1.4	4186	0.056	**9.8E+01**
8400	18	19.2	1.2	4186	0.056	**8.4E+01**
8700	18	19.2	1.2	4186	0.056	**8.4E+01**
9000	18	19.2	1.2	4186	0.056	**8.4E+01**
9300	18	19.2	1.2	4186	0.056	**8.4E+01**
9600	18	19.1	1.1	4186	0.056	**7.7E+01**
9900	18	19.1	1.1	4186	0.056	**7.7E+01**

10200	18	19.1	1.1	4186	0.056	**7.7E+01**
10500	18	19.1	1.1	4186	0.056	**7.7E+01**
10800	18	19.1	1.1	4186	0.056	**7.7E+01**
11100	18	18.9	0.9	4186	0.056	**6.3E+01**
11400	18	18.9	0.9	4186	0.056	**6.3E+01**
11700	18	18.9	0.9	4186	0.056	**6.3E+01**
12000	18	18.9	0.9	4186	0.056	**6.3E+01**
12300	18	18.9	0.9	4186	0.056	**6.3E+01**
12600	18	18.9	0.9	4186	0.056	**6.3E+01**
12900	18	18.6	0.6	4186	0.056	**4.2E+01**
13200	18	18.6	0.6	4186	0.056	**4.2E+01**
13500	18	18.4	0.4	4186	0.056	**2.8E+01**
13800	18	18.2	0.2	4186	0.056	**1.4E+01**
14100	18	18.1	0.1	4186	0.056	**7.0E+00**
14400	18	18.0	0.0	4186	0.056	**0.0E+00**

Table 0.11: Results of RT25 during the discharging phase with a flow rate of 400L/hr

Time(sec)	T_3(°C)	T_4 (°C)	ΔT(°C)	Cp_w(J/kg°C)	Mass flow rate(kg/sec)	Q_2(kJ)
0	18	20.7	2.7	4186	0.112	**379.8**
300	18	20.7	2.7	4186	0.112	**379.8**
600	18	20.6	2.6	4186	0.112	**365.7**
900	18	20.6	2.6	4186	0.112	**365.7**
1200	18	20.6	2.6	4186	0.112	**365.7**
1500	18	20.4	2.4	4186	0.112	**337.6**
1800	18	20.4	2.4	4186	0.112	**337.6**
2100	18	20.3	2.3	4186	0.112	**323.5**
2400	18	20.3	2.3	4186	0.112	**323.5**
2700	18	20.2	2.2	4186	0.112	**309.4**
3000	18	20.2	2.2	4186	0.112	**309.4**
3300	18	20.2	2.2	4186	0.112	**309.4**
3600	18	20.0	2.0	4186	0.112	**281.3**
3900	18	20.0	2.0	4186	0.112	**281.3**
4200	18	20.0	2.0	4186	0.112	**281.3**
4500	18	19.9	1.9	4186	0.112	**267.2**
4800	18	19.8	1.8	4186	0.112	**253.2**

5100	18	19.8	1.8	4186	0.112	**253.2**
5400	18	19.8	1.8	4186	0.112	**253.2**
5700	18	19.8	1.8	4186	0.112	**253.2**
6000	18	19.7	1.7	4186	0.112	**239.1**
6300	18	19.7	1.7	4186	0.112	**239.1**
6600	18	19.7	1.7	4186	0.112	**239.1**
6900	18	19.5	1.5	4186	0.112	**211.0**
7200	18	19.5	1.5	4186	0.112	**211.0**
7500	18	19.4	1.4	4186	0.112	**196.9**
7800	18	19.3	1.3	4186	0.112	**182.8**
8100	18	19.3	1.3	4186	0.112	**182.8**
8400	18	19.3	1.3	4186	0.112	**182.8**
8700	18	19.1	1.1	4186	0.112	**154.7**
9000	18	19.1	1.1	4186	0.112	**154.7**
9300	18	19.1	1.1	4186	0.112	**154.7**
9600	18	19.1	1.1	4186	0.112	**154.7**
9900	18	18.8	0.8	4186	0.112	**112.5**
10200	18	18.8	0.8	4186	0.112	**112.5**
10500	18	18.6	0.6	4186	0.112	**84.4**
10800	18	18.4	0.4	4186	0.112	**56.3**
11100	18	18.3	0.3	4186	0.112	**42.2**
11400	18	18.3	0.3	4186	0.112	**42.2**
11700	18	18.2	0.2	4186	0.112	**28.1**
12000	18	18.0	0.0	4186	0.112	**0.0**

Table 0.12: Results of RT25 during the discharging phase with a flow rate of 600L/hr

Time(sec)	T_3(°C)	T_4 (°C)	ΔT(°C)	Cp_w(J/kg°C)	Mass flow rate(kg/sec)	Q_2(kJ)
0	18	20.5	2.5	4186	0.168	**527.4**
300	18	20.5	2.5	4186	0.168	**527.4**
600	18	20.5	2.5	4186	0.168	**527.4**
900	18	20.5	2.5	4186	0.168	**527.4**
1200	18	20.5	2.5	4186	0.168	**527.4**
1500	18	20.4	2.4	4186	0.168	**506.3**
1800	18	20.3	2.3	4186	0.168	**485.2**
2100	18	20.3	2.3	4186	0.168	**485.2**
2400	18	20.3	2.3	4186	0.168	**485.2**
2700	18	20.3	2.3	4186	0.168	**485.2**
3000	18	20.1	2.1	4186	0.168	**443.0**
3300	18	20.1	2.1	4186	0.168	**443.0**
3600	18	20.1	2.1	4186	0.168	**443.0**
3900	18	20.1	2.1	4186	0.168	**443.0**
4200	18	19.9	1.9	4186	0.168	**400.9**
4500	18	19.9	1.9	4186	0.168	**400.9**
4800	18	19.9	1.9	4186	0.168	**400.9**
5100	18	19.9	1.9	4186	0.168	**400.9**
5400	18	19.8	1.8	4186	0.168	**379.8**
5700	18	19.8	1.8	4186	0.168	**379.8**
6000	18	19.7	1.7	4186	0.168	**358.7**
6300	18	19.7	1.7	4186	0.168	**358.7**
6600	18	19.6	1.6	4186	0.168	**337.6**
6900	18	19.6	1.6	4186	0.168	**337.6**
7200	18	19.6	1.6	4186	0.168	**337.6**
7500	18	19.5	1.5	4186	0.168	**316.5**
7800	18	19.4	1.4	4186	0.168	**295.4**
8100	18	19.4	1.4	4186	0.168	**295.4**
8400	18	19.3	1.3	4186	0.168	**274.3**
8700	18	19.3	1.3	4186	0.168	**274.3**
9000	18	19.3	1.3	4186	0.168	**274.3**
9300	18	19.1	1.1	4186	0.168	**232.1**
9600	18	19.1	1.1	4186	0.168	**232.1**
9900	18	19.1	1.1	4186	0.168	**232.1**

10200	18	19.0	1.0	4186	0.168	**211.0**
10500	18	18.8	0.8	4186	0.168	**168.8**
10800	18	18.0	0.0	4186	0.168	**0.0**

Table 0.13: Results of RT27 during the discharging phase with a flow rate of 200L/hr

Time(sec)	T_3(°C)	T_4 (°C)	ΔT(°C)	Cp_w(J/kg°C)	Mass flow ratekg/sec)	Q_2(kJ)
0	18	20.5	2.5	4186	0.056	**175.8**
300	18	20.5	2.5	4186	0.056	**175.8**
600	18	20.5	2.5	4186	0.056	**175.8**
900	18	20.5	2.5	4186	0.056	**175.8**
1200	18	20.2	2.2	4186	0.056	**154.7**
1500	18	20.2	2.2	4186	0.056	**154.7**
1800	18	20.2	2.2	4186	0.056	**154.7**
2100	18.3	20.4	2.1	4186	0.056	**147.7**
2400	18.3	20.4	2.1	4186	0.056	**147.7**
2700	18	20.1	2.1	4186	0.056	**147.7**
3000	18	20.1	2.1	4186	0.056	**147.7**
3300	18	20.1	2.1	4186	0.056	**147.7**
3600	18	20.0	2.0	4186	0.056	**140.6**
3900	18	20.0	2.0	4186	0.056	**140.6**
4200	18	20.0	2.0	4186	0.056	**140.6**
4500	18	20.0	2.0	4186	0.056	**140.6**
4800	18	20.0	2.0	4186	0.056	**140.6**
5100	18	20.0	2.0	4186	0.056	**140.6**
5400	18	20.0	2.0	4186	0.056	**140.6**
5700	18	19.8	1.8	4186	0.056	**126.6**
6000	18	19.8	1.8	4186	0.056	**126.6**
6300	18	19.8	1.8	4186	0.056	**126.6**
6600	18	19.8	1.8	4186	0.056	**126.6**
6900	18	19.8	1.8	4186	0.056	**126.6**
7200	18	19.8	1.8	4186	0.056	**126.6**
7500	18	19.8	1.8	4186	0.056	**126.6**
7800	18	19.5	1.5	4186	0.056	**105.5**
8100	18	19.5	1.5	4186	0.056	**105.5**
8400	18	19.5	1.5	4186	0.056	**105.5**

8700	18	19.5	1.5	4186	0.056	**105.5**
9000	18	19.3	1.3	4186	0.056	**91.4**
9300	18	19.3	1.3	4186	0.056	**91.4**
9600	18	19.3	1.3	4186	0.056	**91.4**
9900	18	19.1	1.1	4186	0.056	**77.4**
10200	18	19.1	1.1	4186	0.056	**77.4**
10500	18	19.1	1.1	4186	0.056	**77.4**
10800	18	19.1	1.1	4186	0.056	**77.4**
11100	18	19.1	1.1	4186	0.056	**77.4**
11400	18	19.0	1.0	4186	0.056	**70.3**
11700	18	19.0	1.0	4186	0.056	**70.3**
12000	18	19.0	1.0	4186	0.056	**70.3**
12300	18	19.0	1.0	4186	0.056	**70.3**
12600	18	19.0	1.0	4186	0.056	**70.3**
12900	18	18.8	0.8	4186	0.056	**56.3**
13200	18	18.8	0.8	4186	0.056	**56.3**
13500	18	18.8	0.8	4186	0.056	**56.3**
13800	18	18.7	0.7	4186	0.056	**49.2**
14100	18	18.7	0.7	4186	0.056	**49.2**
14400	18	18.7	0.7	4186	0.056	**49.2**
14700	18	18.7	0.7	4186	0.056	**49.2**
15000	18	18.5	0.5	4186	0.056	**35.2**
15300	18	18.4	0.4	4186	0.056	**28.1**
15600	18	18.2	0.2	4186	0.056	**14.1**
15900	18	18.0	0.0	4186	0.056	**0.0**

Table 0.14: Results of RT27 during the discharging phase with a flow rate of 400L/hr

Time(sec)	T_3(°C)	T_4 (°C)	ΔT(°C)	Cp_w(J/kg°C)	Mass flow rate(kg/sec)	Q_2(kJ)
0	18	20.8	2.8	4186	0.112	**393.8**
300	18	20.8	2.8	4186	0.112	**393.8**
600	18	20.8	2.8	4186	0.112	**393.8**
900	18	20.8	2.8	4186	0.112	**393.8**
1200	18	20.8	2.8	4186	0.112	**393.8**
1500	18	20.7	2.7	4186	0.112	**379.8**
1800	18	20.7	2.7	4186	0.112	**379.8**
2100	18	20.7	2.7	4186	0.112	**379.8**
2400	18	20.7	2.7	4186	0.112	**379.8**
2700	18	20.6	2.6	4186	0.112	**365.7**
3000	18	20.6	2.6	4186	0.112	**365.7**
3300	18	20.6	2.6	4186	0.112	**365.7**
3600	18	20.3	2.3	4186	0.112	**323.5**
3900	18	20.3	2.3	4186	0.112	**323.5**
4200	18	20.3	2.3	4186	0.112	**323.5**
4500	18	20.3	2.3	4186	0.112	**323.5**
4800	18	20.3	2.3	4186	0.112	**323.5**
5100	18	20.3	2.3	4186	0.112	**323.5**
5400	18	19.9	1.9	4186	0.112	**267.2**
5700	18	19.9	1.9	4186	0.112	**267.2**
6000	18	19.9	1.9	4186	0.112	**267.2**
6300	18	19.7	1.7	4186	0.112	**239.1**
6600	18	19.7	1.7	4186	0.112	**239.1**
6900	18	19.7	1.7	4186	0.112	**239.1**
7200	18	19.4	1.4	4186	0.112	**196.9**
7500	18	19.4	1.4	4186	0.112	**196.9**
7800	18	19.4	1.4	4186	0.112	**196.9**
8100	18	19.4	1.4	4186	0.112	**196.9**
8400	18	19.2	1.2	4186	0.112	**168.8**
8700	18	19.2	1.2	4186	0.112	**168.8**
9000	18	19.2	1.2	4186	0.112	**168.8**
9300	18	19.2	1.2	4186	0.112	**168.8**
9600	18	19.0	1.0	4186	0.112	**140.6**
9900	18	19.0	1.0	4186	0.112	**140.6**

10200	18	19.0	1.0	4186	0.112	**140.6**
10500	18	19.0	1.0	4186	0.112	**140.6**
10800	18	18.8	0.8	4186	0.112	**112.5**
11100	18	18.8	0.8	4186	0.112	**112.5**
11400	18	18.8	0.8	4186	0.112	**112.5**
11700	18	18.8	0.8	4186	0.112	**112.5**
12000	18	18.6	0.6	4186	0.112	**84.4**
12300	18	18.6	0.6	4186	0.112	**84.4**
12600	18	18.5	0.5	4186	0.112	**70.3**
12900	18	18.5	0.5	4186	0.112	**70.3**
13200	18	18.3	0.3	4186	0.112	**42.2**
13500	18	18.0	0.0	4186	0.112	**0.0**
13800	18	18.0	0.0	4186	0.112	**0.0**

Table 0.15: Results of RT27 during the discharging phase with a flow rate of 600L/hr

Time(sec)	T_3(°C)	T_4 (°C)	ΔT(°C)	Cp_w(J/kg°C)	Mass flow rate(kg/sec)	Q_2(kJ)
0	18.0	20.9	2.9	4186	0.168	**611.8**
300	18.0	20.9	2.9	4186	0.168	**611.8**
600	18.0	20.9	2.9	4186	0.168	**611.8**
900	18.0	20.8	2.8	4186	0.168	**590.7**
1200	18.0	20.8	2.8	4186	0.168	**590.7**
1500	18.0	20.8	2.8	4186	0.168	**590.7**
1800	18.0	20.7	2.7	4186	0.168	**569.6**
2100	18.0	20.7	2.7	4186	0.168	**569.6**
2400	18.0	20.6	2.6	4186	0.168	**548.5**
2700	18.0	20.6	2.6	4186	0.168	**548.5**
3000	18.0	20.5	2.5	4186	0.168	**527.4**
3300	18.0	20.5	2.5	4186	0.168	**527.4**
3600	18.0	20.5	2.5	4186	0.168	**527.4**
3900	18.0	20.4	2.4	4186	0.168	**506.3**
4200	18.0	20.4	2.4	4186	0.168	**506.3**
4500	18.0	20.4	2.4	4186	0.168	**506.3**
4800	18.0	20.3	2.3	4186	0.168	**485.2**
5100	18.0	20.3	2.3	4186	0.168	**485.2**
5400	18.0	20.3	2.3	4186	0.168	**485.2**
5700	18.0	20.2	2.2	4186	0.168	**464.1**

6000	18.0	20.1	2.1	4186	0.168	**443.0**
6300	18.0	20.1	2.1	4186	0.168	**443.0**
6600	18.0	20.1	2.1	4186	0.168	**443.0**
6900	18.0	20.0	2.0	4186	0.168	**421.9**
7200	18.0	20.0	2.0	4186	0.168	**421.9**
7500	18.0	20.0	2.0	4186	0.168	**421.9**
7800	18.0	20.0	2.0	4186	0.168	**421.9**
8100	18.0	19.8	1.8	4186	0.168	**379.8**
8400	18.0	19.8	1.8	4186	0.168	**379.8**
8700	18.0	19.7	1.7	4186	0.168	**358.7**
9000	18.0	19.6	1.6	4186	0.168	**337.6**
9300	18.0	19.5	1.5	4186	0.168	**316.5**
9600	18.0	19.5	1.5	4186	0.168	**316.5**
9900	18.0	19.4	1.4	4186	0.168	**295.4**
10200	18.0	19.4	1.4	4186	0.168	**295.4**
10500	18.0	19.3	1.3	4186	0.168	**274.3**
10800	18.0	19.2	1.2	4186	0.168	**253.2**
11100	18.0	19.2	1.2	4186	0.168	**253.2**
11400	18.0	19.0	1.0	4186	0.168	**211.0**
11700	18.0	19.0	1.0	4186	0.168	**211.0**
12000	18.0	18.7	0.7	4186	0.168	**147.7**
12300	18.0	18.0	0.0	4186	0.168	**0.0**

Table 0.16: Results of RT35 during the discharging phase with a flow rate of 200L/hr

Time(sec)	T_3 (°C)	T_4 (°C)	ΔT(°C)	Cp_w(J/kg°C)	Mass flow rate(kg/sec)	Q_2(kJ)
0	18.0	20.8	2.8	4186	0.056	**196.9**
300	18.0	20.7	2.7	4186	0.056	**189.9**
600	18.0	20.7	2.7	4186	0.056	**189.9**
900	18.0	20.7	2.7	4186	0.056	**189.9**
1200	18.0	20.7	2.7	4186	0.056	**189.9**
1500	18.0	20.6	2.6	4186	0.056	**182.8**
1800	18.0	20.6	2.6	4186	0.056	**182.8**
2100	18.0	20.6	2.6	4186	0.056	**182.8**
2400	18.0	20.4	2.4	4186	0.056	**168.8**
2700	18.0	20.4	2.4	4186	0.056	**168.8**

3000	18.0	20.4	2.4	4186	0.056	**168.8**
3300	18.0	20.4	2.4	4186	0.056	**168.8**
3600	18.2	20.6	2.4	4186	0.056	**168.8**
3900	18.0	20.3	2.3	4186	0.056	**161.7**
4200	18.0	20.3	2.3	4186	0.056	**161.7**
4500	18.0	20.2	2.2	4186	0.056	**154.7**
4800	18.0	20.2	2.2	4186	0.056	**154.7**
5100	18.0	20.2	2.2	4186	0.056	**154.7**
5400	18.0	20.2	2.2	4186	0.056	**154.7**
5700	18.0	20.2	2.2	4186	0.056	**154.7**
6000	18.0	20.1	2.1	4186	0.056	**147.7**
6300	18.0	20.1	2.1	4186	0.056	**147.7**
6600	18.0	20.1	2.1	4186	0.056	**147.7**
6900	18.0	20.1	2.1	4186	0.056	**147.7**
7200	18.0	20.1	2.1	4186	0.056	**147.7**
7500	18.0	20.1	2.1	4186	0.056	**147.7**
7800	18.0	20.0	2.0	4186	0.056	**140.6**
8100	18.0	20.0	2.0	4186	0.056	**140.6**
8400	18.0	20.0	2.0	4186	0.056	**140.6**
8700	18.0	20.0	2.0	4186	0.056	**140.6**
9000	18.0	19.9	1.9	4186	0.056	**133.6**
9300	18.0	19.9	1.9	4186	0.056	**133.6**
9600	18.0	19.9	1.9	4186	0.056	**133.6**
9900	18.0	19.8	1.8	4186	0.056	**126.6**
10200	18.0	19.8	1.8	4186	0.056	**126.6**
10500	18.0	19.8	1.8	4186	0.056	**126.6**
10800	18.0	19.8	1.8	4186	0.056	**126.6**
11100	18.0	19.8	1.8	4186	0.056	**126.6**
11400	18.0	19.8	1.8	4186	0.056	**126.6**
11700	18.0	19.7	1.7	4186	0.056	**119.6**
12000	18.0	19.7	1.7	4186	0.056	**119.6**
12300	18.0	19.6	1.6	4186	0.056	**112.5**
12600	18.0	19.6	1.6	4186	0.056	**112.5**
12900	18.0	19.6	1.6	4186	0.056	**112.5**
13200	18.0	19.6	1.6	4186	0.056	**112.5**
13500	18.0	19.6	1.6	4186	0.056	**112.5**

13800	18.0	19.6	1.6	4186	0.056	**112.5**
14100	18.0	19.5	1.5	4186	0.056	**105.5**
14400	18.0	19.4	1.4	4186	0.056	**98.5**
14700	18.0	19.2	1.2	4186	0.056	**84.4**
15000	18.0	19.0	1.0	4186	0.056	**70.3**
15300	18.0	18.9	0.9	4186	0.056	**63.3**
15600	18.0	18.7	0.7	4186	0.056	**49.2**
15900	18.0	18.5	0.5	4186	0.056	**35.2**
16200	18.0	18.5	0.5	4186	0.056	**35.2**
16500	18.0	18.5	0.5	4186	0.056	**35.2**
16800	18.0	18.4	0.4	4186	0.056	**28.1**
17100	18.0	18.3	0.3	4186	0.056	**21.1**
17400	18.0	18.2	0.2	4186	0.056	**14.1**
17700	18.0	18.1	0.1	4186	0.056	**7.0**
18000	18.0	18.0	0.0	4186	0.056	**0.0**

Table 0.17: Results of RT35 during the discharging phase with a flow rate of 400L/hr

Time(sec)	T_3 (°C)	T_4 (°C)	ΔT(°C)	Cp_w(J/kg°C)	Mass flow rate(kg/sec)	Q_2(kJ)
0	18.0	21.1	3.1	4186	0.112	**436.0**
300	18.0	21.1	3.1	4186	0.112	**436.0**
600	18.0	21.1	3.1	4186	0.112	**436.0**
900	18.0	21.0	3.0	4186	0.112	**421.9**
1200	18.0	21.0	3.0	4186	0.112	**421.9**
1500	18.0	20.8	2.8	4186	0.112	**393.8**
1800	18.0	20.8	2.8	4186	0.112	**393.8**
2100	18.0	20.8	2.8	4186	0.112	**393.8**
2400	18.0	20.8	2.8	4186	0.112	**393.8**
2700	18.0	20.7	2.7	4186	0.112	**379.8**
3000	18.0	20.7	2.7	4186	0.112	**379.8**
3300	18.0	20.7	2.7	4186	0.112	**379.8**
3600	18.0	20.5	2.5	4186	0.112	**351.6**
3900	18.0	20.5	2.5	4186	0.112	**351.6**
4200	18.0	20.5	2.5	4186	0.112	**351.6**
4500	18.0	20.4	2.4	4186	0.112	**337.6**

4800	18.0	20.4	2.4	4186	0.112	**337.6**
5100	18.0	20.4	2.4	4186	0.112	**337.6**
5400	18.0	20.2	2.2	4186	0.112	**309.4**
5700	18.0	20.2	2.2	4186	0.112	**309.4**
6000	18.0	20.2	2.2	4186	0.112	**309.4**
6300	18.0	20.0	2.0	4186	0.112	**281.3**
6600	18.0	20.0	2.0	4186	0.112	**281.3**
6900	18.0	20.0	2.0	4186	0.112	**281.3**
7200	18.0	20.0	2.0	4186	0.112	**281.3**
7500	18.0	20.0	2.0	4186	0.112	**281.3**
7800	18.0	19.9	1.9	4186	0.112	**267.2**
8100	18.0	19.9	1.9	4186	0.112	**267.2**
8400	18.0	19.9	1.9	4186	0.112	**267.2**
8700	18.0	19.8	1.8	4186	0.112	**253.2**
9000	18.0	19.8	1.8	4186	0.112	**253.2**
9300	18.0	19.8	1.8	4186	0.112	**253.2**
9600	18.0	19.6	1.6	4186	0.112	**225.0**
9900	18.0	19.6	1.6	4186	0.112	**225.0**
10200	18.0	19.5	1.5	4186	0.112	**211.0**
10500	18.0	19.5	1.5	4186	0.112	**211.0**
10800	18.0	19.5	1.5	4186	0.112	**211.0**
11100	18.0	19.5	1.5	4186	0.112	**211.0**
11400	18.0	19.5	1.5	4186	0.112	**211.0**
11700	18.0	19.5	1.5	4186	0.112	**211.0**
12000	18.0	19.5	1.5	4186	0.112	**211.0**
12300	18.0	19.4	1.4	4186	0.112	**196.9**
12600	18.0	19.4	1.4	4186	0.112	**196.9**
12900	18.0	19.3	1.3	4186	0.112	**182.8**
13200	18.0	19.3	1.3	4186	0.112	**182.8**
13500	18.0	19.3	1.3	4186	0.112	**182.8**
13800	18.0	19.3	1.3	4186	0.112	**182.8**
14100	18.0	19.2	1.2	4186	0.112	**168.8**
14400	18.0	19.3	1.3	4186	0.112	**182.8**
14700	18.0	19.2	1.2	4186	0.112	**168.8**
15000	18.0	19.2	1.2	4186	0.112	**168.8**
15300	18.0	18.9	0.9	4186	0.112	**126.6**

15600	18.0	18.8	0.8	4186	0.112	**112.5**
15900	18.0	18.0	0.0	4186	0.112	**0.0**

Table 0.18: Results of RT35 during the discharging phase with a flow rate of 600L/hr

Time(sec)	T_3(°C)	T_4 (°C)	ΔT(°C)	Cp_w(J/kg°C)	Mass flow rate(kg/sec)	Q_2(kJ)
0	18.0	21.3	3.3	4186	0.168	**696.2**
300	18.0	21.3	3.3	4186	0.168	**696.2**
600	18.0	21.2	3.2	4186	0.168	**675.1**
900	18.0	21.1	3.1	4186	0.168	**654.0**
1200	18.0	21.1	3.1	4186	0.168	**654.0**
1500	18.0	21.1	3.1	4186	0.168	**654.0**
1800	18.0	20.9	2.9	4186	0.168	**611.8**
2100	18.0	20.9	2.9	4186	0.168	**611.8**
2400	18.0	20.9	2.9	4186	0.168	**611.8**
2700	18.0	20.8	2.8	4186	0.168	**590.7**
3000	18.0	20.8	2.8	4186	0.168	**590.7**
3300	18.0	20.6	2.6	4186	0.168	**548.5**
3600	18.0	20.6	2.6	4186	0.168	**548.5**
3900	18.0	20.6	2.6	4186	0.168	**548.5**
4200	18.0	20.6	2.6	4186	0.168	**548.5**
4500	18.0	20.4	2.4	4186	0.168	**506.3**
4800	18.0	20.4	2.4	4186	0.168	**506.3**
5100	18.0	20.4	2.4	4186	0.168	**506.3**
5400	18.0	20.4	2.4	4186	0.168	**506.3**
5700	18.0	20.4	2.4	4186	0.168	**506.3**
6000	18.0	20.3	2.3	4186	0.168	**485.2**
6300	18.0	20.3	2.3	4186	0.168	**485.2**
6600	18.0	20.1	2.1	4186	0.168	**443.0**
6900	18.0	20.0	2.0	4186	0.168	**421.9**
7200	18.0	20.0	2.0	4186	0.168	**421.9**
7500	18.0	20.0	2.0	4186	0.168	**421.9**
7800	18.0	20.0	2.0	4186	0.168	**421.9**
8100	18.0	20.0	2.0	4186	0.168	**421.9**
8400	18.0	20.0	2.0	4186	0.168	**421.9**
8700	18.0	19.8	1.8	4186	0.168	**379.8**

9000	18.0	19.8	1.8	4186	0.168	**379.8**
9300	18.0	19.8	1.8	4186	0.168	**379.8**
9600	18.0	19.8	1.8	4186	0.168	**379.8**
9900	18.0	19.6	1.6	4186	0.168	**337.6**
10200	18.0	19.6	1.6	4186	0.168	**337.6**
10500	18.0	19.6	1.6	4186	0.168	**337.6**
10800	18.0	19.4	1.4	4186	0.168	**295.4**
11100	18.0	19.4	1.4	4186	0.168	**295.4**
11400	18.0	19.4	1.4	4186	0.168	**295.4**
11700	18.0	19.4	1.4	4186	0.168	**295.4**
12000	18.0	19.2	1.2	4186	0.168	**253.2**
12300	18.0	19.2	1.2	4186	0.168	**253.2**
12600	18.0	19.2	1.2	4186	0.168	**253.2**
12900	18.0	19.0	1.0	4186	0.168	**211.0**
13200	18.0	19.0	1.0	4186	0.168	**211.0**
13500	18.0	18.9	0.9	4186	0.168	**189.9**
13800	18.0	18.6	0.6	4186	0.168	**126.6**
14100	18.0	18.3	0.3	4186	0.168	**63.3**
14400	18.0	18.3	0.3	4186	0.168	**63.3**
14700	18.0	18.0	0.0	4186	0.168	**0.0**